TECHNICAL REPORT
W-6382 1/22/02

BROOKHAVEN NATIONAL LABORATORY

Studies of the Rod Ejection Accident in a PWR

D.J. Diamond, B.P. Bromley, and A.L. Aronson

January 22, 2002

Energy Sciences & Technology Dept.
Brookhaven National Laboratory
Brookhaven Science Associates
Upton, New York, 11973-5000

Prepared for the U.S. Nuclear Regulatory Commission
Office of Nuclear Regulatory Research
Contract No. DE-AC-02-98CH10886

Studies of the Rod Ejection Accident in a PWR

D.J. Diamond, B.P. Bromley, and A.L. Aronson
Brookhaven National Laboratory
Upton, New York, 11973

January 22, 2002

Prepared for the U.S. Nuclear Regulatory Commission
Washington, D.C. 20555
Contract No. DE-AC-02-98CH10886
FIN W-6382

ABSTRACT

This report documents the results of a series of parametric studies of a control rod ejection accident (REA) using a model of the core of the Three Mile Island Unit 1 (TMI-1) pressurized water reactor. Base cases are from a hot zero power (HZP) condition at both the end and beginning of a typical fuel cycle. PARCS, a transient, three-dimensional, two-group neutron diffusion code, coupled with its own thermal-hydraulics model, is used to perform the simulations. Super-prompt-critical REAs are simulated by artificially increasing the worth of the ejected rod using multiplication factors on the cross sections within the fuel assembly containing the ejected control rod. The maximum specific energy deposition in the fuel as a result of the power pulse caused by an REA is correlated against ejected rod worth and delayed neutron fraction which are the two most important global parameters. In addition, sensitivity studies look at heat transfer properties, power level and reactor trip. Results show that for the nominal case, the peak fuel pellet enthalpy increase is less than 40 cal/g for a $1.5 ejected rod and less than 70 cal/g for a $2.0 rod. The pulse width for an REA ranges from 65 ms to 10 ms for peak fuel enthalpy changes from 15 cal/g to 100 cal/g. This suggests that experiments to test the limits of energy deposition should be done with pulse widths of ~10 ms. The energy deposition at beginning-of-cycle (BOC) tends to be higher than at end-of-cycle for the same rod worth due to the higher fissile content in the fuel at BOC. The energy deposition at HZP is greater than at elevated power due to the decrease in rod worth with both power level and the withdrawal of control rods concomitant with elevated power. The trends shown in the quite rigorous PARCS core simulation are remarkably similar to those suggested by the approximate analytical Nordheim-Fuchs model.

CONTENTS

ACKNOWLEDGEMENTS

The authors wish to thank Dr. H. Joo of the Korean Atomic Energy Research Institute and Professor T. Downar of Purdue University for their technical support in the use of the PARCS code. Thanks are also extended to Prof. K. Ivanov at Pennsylvania State University for providing the specifications and cross section data for the models of the TMI-1 core. The authors appreciate getting independent calculational results from Drs. A. Avvakumov and V. Malofeev at the Russian Research Centre - Kurchatov Institute, which helped assure the validity of the calculations done for this study. Finally, the authors thank Ms. S. Monteleone for assistance in the preparation of this report.

LIST OF FIGURES

LIST OF TABLES

1. INTRODUCTION

1.1 Background

The rod ejection accident (REA) is the design-basis reactivity-initiated accident in pressurized water reactors (PWRs). It is based on assuming that there is a mechanical failure of the housing of a control rod drive mechanism so that the internal pressure in the core forces the mechanism out and the attached control rod assembly is ejected. The complete withdrawal of a control rod, which takes place in approximately 100 ms, results in a positive reactivity insertion that causes a power surge in the core. If the ejected rod worth is above prompt-critical ($1), the power surge will grow rapidly. Although the power surge will be limited by negative fuel temperature (Doppler) feedback, significant energy deposition in the fuel may occur during the event which is eventually terminated by reactor trip. The expected frequency of occurrence of an REA is less than 1.0E-6/reactor-year [1] although this estimate does not take into account recent evidence of cracking which is currently under investigation.

The acceptance criterion, to avoid unacceptable fuel damage during the event, is a local fuel enthalpy, radially averaged across the pellet, of less than 280 cal/g. Departure from nucleate boiling (DNB) has been used as an indicator of when ("acceptable") fuel damage occurs for the purpose of assessing radiological consequences for which there are other acceptance criteria. This event has been analyzed for the licensing of all PWRs and results have always shown that the acceptance criteria are met with considerable margin.

There has been recent interest in the REA as a result of experiments in France and Japan which have shown that unacceptable fuel damage may occur at fuel enthalpies much lower than the current acceptance criterion (280 cal/g). These experiments are with fuel with considerable burnup whereas the 280 cal/g criterion was based on data primarily for fresh fuel. The implication of this is a need for a more stringent acceptance criterion. In turn, this has led analysts to perform best-estimate calculations which reconfirm the large safety margin implicit when using the conservative methods traditionally used for licensing calculations.

The U.S. Nuclear Regulatory Commission (NRC) has been studying the impact of burnup on the consequences of the REA through a varied research program which includes support for a) experiments in which fuel pellets are subjected to energy depositions similar to those expected during an REA, b) mechanical testing of cladding specimens, and c) calculations of fuel response to an REA. The latter includes the use of coupled neutronic and thermal-hydraulic codes as well as fuel behavior codes. These studies are intended to help define new acceptance criteria for the REA as well as to further our understanding of the design-basis accident. As a result of these efforts, it has been proposed that the acceptance criterion may be as low as 100 cal/g [2].

Brookhaven National Laboratory (BNL) has been tasked with the responsibility to do coupled neutronic and thermal-hydraulic calculations of the REA in order to understand the effect of a) reactor conditions on the fuel enthalpy, b) the uncertainty in fuel enthalpy that would be relevant to licensing calculations carried out with best-estimate methods, and c) the characteristics of the power pulse so that the corresponding experiments would be prototypical. Some of this effort has been coordinated with studies, supported by the NRC, at the Russian Research Centre - Kurchatov Institute (RRC-KI)

This report is one of several that have been written to meet these objectives. It complements reports written in the past that focus on sensitivity studies [3,4], validation of methods [5], and uncertainty analysis [6].

1.2 Objectives

The original objective of this project was to investigate the important parameters which influence the energy deposition (approximately equal to the increase in fuel enthalpy) during an REA to determine if there were steady state core parameters which define the consequences. If this were the case it would negate the necessity of doing transient analysis for every fuel cycle in order to assess compliance with the acceptance criteria. For example, it is already well-known that if the ejected rod worth is less than $1 then there is no prompt-critical excursion and the fuel enthalpy increase will be limited. Hence, one could use this limit on rod worth in lieu of doing a transient analysis of the REA and calculating fuel enthalpy. This example, however, is flawed in that some reactor designs result in rod worths greater than $1.

With that objective in mind, parametric studies were carried out varying the rod worth and delayed neutron fraction as these were expected to be the two most important parameters in determining energy deposition. As these studies were being done, other parameters were recognized as being important and needing study. Hence this study looked at the effect on fuel enthalpy of the following:

- rod worth
- delayed neutron fraction
- the position of the ejected rod
- the time during the fuel cycle (beginning- vs end-of-cycle)
- power level (hot zero power vs low power)
- fuel heat capacity
- gap conductance
- pellet power distribution
- reactor trip

The study also looked at the correlation between energy deposition and pulse width. The objective in this part of the study was to supply information which could be used in the design of new experiments wherein fuel pellet samples would be subjected to power pulses in order to determine fuel behavior.

1.3 Scope and Organization of this Report

This report describes studies of pulse width and fuel enthalpy for a hypothetical REA. A description of the calculational methodology for these studies is found in Section 2. This includes a discussion of the PARCS core dynamics code, the reactor model of Three Mile Island Unit 1 (TMI-1), the types of parametric studies performed, and comparisons made with analysis done at RRC-KI. The results of the various REA simulations are discussed in Section 3. Conclusions and recommendations are given in Section 4.

2. CALCULATIONAL METHODOLOGY

2.1 PARCS Reactor Dynamics Simulation Code

The PARCS (Purdue Advanced Reactor Core Simulator) code (Version 1.05) [7] was used to simulate both the steady-state and transient reactor behavior of the TMI-1 core. PARCS is a three-dimensional, two-group diffusion model using nodal methods. It has been coupled to the thermal-hydraulics codes RELAP5 and TRAC-M but for the present study a stand-alone version has been used which incorporates a simpler thermal-hydraulics model. It was confirmed, by doing sample comparsions, that this model provides the same level of accuracy for an REA calculation as use of PARCS/RELAP5. This occurs because the difference in codes is primarily in fluid dynamics modeling and this does not have a strong impact on the REA.

2.2 PARCS Model of TMI-1

Some of the design and operational parameters of the TMI-1 core model [8] at end-of cycle (EOC), as well as nodalization in PARCS are given in Table 2.1. Figure 2.1 is the core layout showing the 177 fuel assemblies and the positions of Control Banks 1-8. There are four radial neutronic nodes per fuel or reflector assembly, giving a total of 964 radial nodes. There are 28 axial neutronic nodes. There is one thermal-hydraulic (TH) channel node per fuel assembly. Banks 1, 2, 3, and 4 are safety banks that are inserted to shut down the reactor in the event of a reactor trip or a planned shut down. Banks 5, 6, and 7 are regulating banks that are used to adjust the power level. Bank 8 contains axial power-shaping rods (APSRs). In the transient analysis of a rod ejection accident (REA), the control rod assembly in the center of the core, 7A, is ejected. For some studies, control rods 7B or 7C were assumed ejected.

For beginning-of-cycle (BOC) calculations the only parameters in Table 2.1 that change are the delayed neutron fraction, which becomes 0.006323, the boron concentration (1700 ppm) and the initial position of Bank 8 which is partially inserted to 291.3 steps.

The version of PARCS in use for the analysis of the TMI-1 core makes use of a table look-up method for obtaining macroscopic cross section data in two energy groups at various fuel temperatures, moderator densities, and boron concentrations within fuel assemblies of a specified composition. The core is modeled with 438 different compositions for unrodded fuel assemblies, and a smaller number of compositions for rodded fuel assemblies. Each composition represents the effect of fuel design, burnable poison history, burnup and moderator density history. The cross section data was generated using the CASMO™ lattice physics code. The preparation and format of the cross section data for the macroscopic cross section data file at BOC differ somewhat from that at EOC. The data at EOC is generated for a specific boron concentration (5 ppm), and the assembly discontinuity factors are directly incorporated into the values of the cross sections. The data at BOC is generated for two values of boron concentration (5 ppm and 2000 ppm), and the assembly discontinuity factors are separated from the cross section data providing a more accurate model.

Table 2.1 Specifications for the PARCS Model for TMI-1

Fuel Cycle	EOC
Full Power Level (FP)	2772 MWth
Hot Zero Power (HZP) Level	1.0E-4 % FP
Number of Fuel Assemblies (FA)	177
Number of Reflector Assemblies	64
Fuel Assembly Size and Pitch	21.8 cm
Active Core Height	357.1 cm
Thickness of Reflector	21.8 cm
Position of Fully Inserted Control Rod Relative to Bottom of Reflector	36.2 cm
Step Size for Control Rods	0.353 cm
Delayed Neutron Fraction (Beta)	0.005211
Number of Delayed Groups	6
Boron Concentration	5 ppm
Inlet Coolant Temperature	278°C
Inlet Coolant Flow per Fuel Assembly	89.5 kg/s
Number of Radial Neutronic Nodes	964
Number of Axial Neutronic Nodes	28 (26 core, 2 reflectors)
Number of Radial TH Nodes	177 (core only)
Number of Axial TH Nodes	26 (core only)
Initial Position for Banks 1 to 4	Withdrawn (971 steps)
Initial Position for Banks 5,6,7	Inserted (0 steps)
Initial Position for Bank 8 (APSR)	Withdrawn (971 steps)

2.3 Rod Ejection Accident Analysis

PARCS is used to calculate a 3-second transient simulation of the core neutronics and thermal-hydraulics behavior during and after the control rod in the central fuel assembly (Rod 7A) is withdrawn in 100 ms. This simulates a rod ejection accident. The withdrawal rate of the control rod is constant. The reactor is set to trip when it reaches 112% of full power (full power is 2772 MWth), with a 400 ms delay between the trip signal and the beginning of the insertion of shutdown control banks 1, 2, 3, and 4. The shutdown banks are inserted at a constant rate, and take 2.2 s to be fully inserted into the core. There is a lower trip setpoint that is set administratively during startup. However, in licensing analysis this trip is ignored since the excore calibration could be from the previous cycle and therefore, inaccurate.

A diagnostic procedure is used in PARCS to find the maximum fuel pellet temperature and fuel pellet enthalpy. The fuel pellet temperature is obtained for each axial node by averaging the pellet temperature radially. The fuel enthalpy is that for uranium dioxide (UO_2) relative to its value at 300 K (27°C) and is obtained using a polynomial which approximates the data found in the MATPRO library of material properties for UO_2 [9].

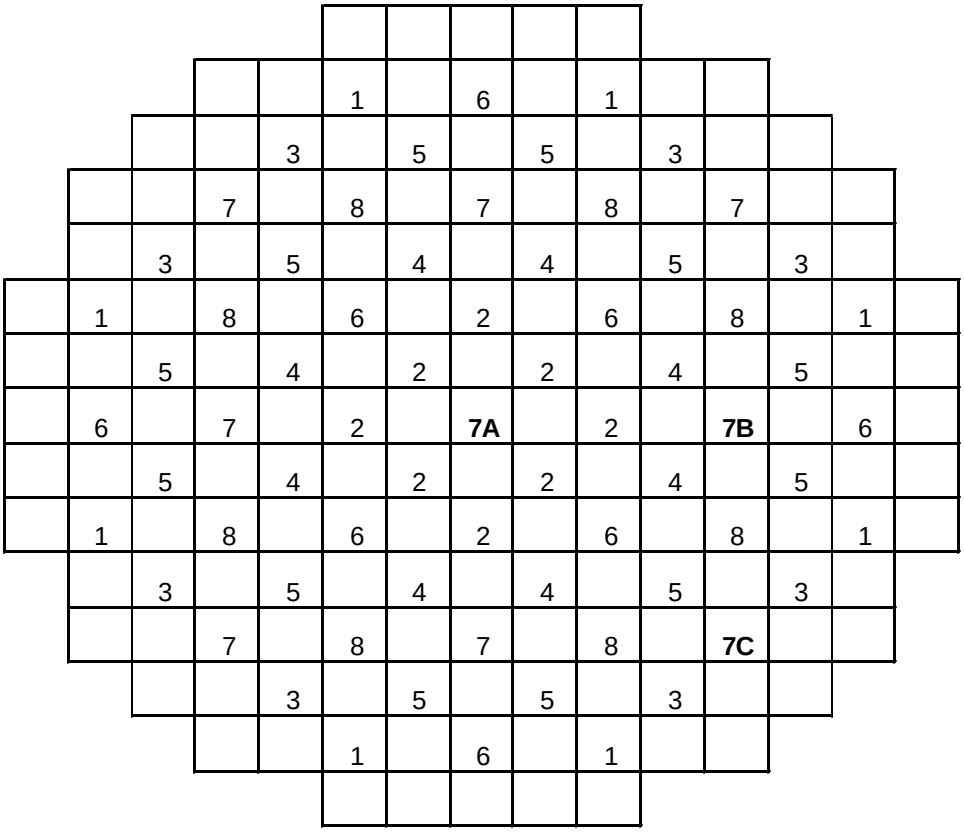

Figure 2.1 Radial arrangement of control rod banks in TMI-1 PWR core

The fuel and moderator density distributions and macroscopic cross sections in the TMI-1 core at EOC and BOC are such that rod 7A has a worth of approximately \$0.66 and \$0.39 respectively at HZP. These control rod worths lead to REAs that are below prompt-critical. Since the goal is to study REA events above prompt critical, the worth of rod 7A is artificially adjusted by changing the macroscopic absorption ($Ó_a$) and fission yield ($õÓ_f$) cross sections in the central fuel assembly when rod 7A is inserted or removed, respectively. The multiplication factor for the absorption cross sections typically varies from 1.0 (no change) to 2.0. The multiplication factor for the fission yield cross sections typically varies from 1.0 (no change) to 1.25. For example, with a multiplication factor 2.0 on the absorption cross section, and a multiplication factor of 1.0 on the fission yield cross section, a rod worth of \$1.22 can be obtained in the EOC HZP case. This expedient for obtaining large rod worths eliminates the time-consuming process of searching for control rod patterns and/or xenon distributions which might lead to those worths.

The total reactivity of the reactor core during the transient is computed using the instantaneous neutron flux distributions and lattice physics parameters based on the composition of each fuel assembly, the instantaneous moderator/coolant density, and the Doppler/fuel temperature. The total reactivity is comprised of several components, including the control reactivity, the Doppler feedback reactivity, and the moderator feedback

reactivity. In the TMI-1 core, the Doppler and moderator feedback reactivity coefficients are negative; therefore, the reactivity due to the fuel and moderator will decrease with rising temperatures. At the beginning of an REA when control rod 7A is fully withdrawn in 100 ms, the Doppler and moderator feedback components are quite small and the control reactivity is approximately the same as the total reactivity.

2.4 Steady State Results

Steady state calculations were carried out to compare with results from other sources as a means of partially validating the model. Steady-state results for the control rod worths at EOC, HZP are shown in Table 2.2 with comparisons to earlier calculations done at BNL with the coupled PARCS/RELAP5 code and by Russian colleagues at RRC-KI using the coupled BARS/RELAP5 code [4,5]. The results for Banks 5-7 are with the banks with lower bank numbers withdrawn (e.g., Bank 6 worth is with Banks 1-5 withdrawn). The results for individual rods within Bank 7 are with Banks 5-7 inserted.

As seen in Table 2.2, there is very little difference between using PARCS as a stand-alone code and PARCS/RELAP5 for steady state analysis at EOC. (Dynamic results are given in Section 3.8.) Since PARCS can be run much more quickly without coupling it to RELAP5, it was, therefore, the basis for all other calculations in this study. The PARCS predictions for rod worths were found to be less than those computed by BARS/RELAP5, differing from 2 to 10%, except for Rod 7C, where the difference was as much as 27%. This large discrepancy may be attributed to the fact that Rod 7C is located close to the reflector, and the treatment of the boundary conditions at the reflector by PARCS is different from BARS. The normalized radial power distributions at EOC HZP with Banks 5,6, and 7 inserted, is shown in Figure 2.2, taking advantage of the one-eight symmetry of the core.

Table 2.2 Steady-State Rod Worth Calculations for TMI-1 at EOC, HZP

TMI-1 PWR EOC HZP					
Rod or Bank	PARCS Stand Alone Rod Worth (pcm)	PARCS RELAP-5 Rod Worth (pcm)	Difference (%)	BARS RELAP-5 Rod Worth (pcm)	Difference (%)
5	1422	1423	-0.05	1524	-6.7
6	848	849	-0.13	868	-2.3
7	1048	1050	-0.16	1085	-3.4
7a	346	347	-0.37	372	-7.1
7b	188	188	-0.18	208	-9.8
7c	345	344	0.43	473	-27.0

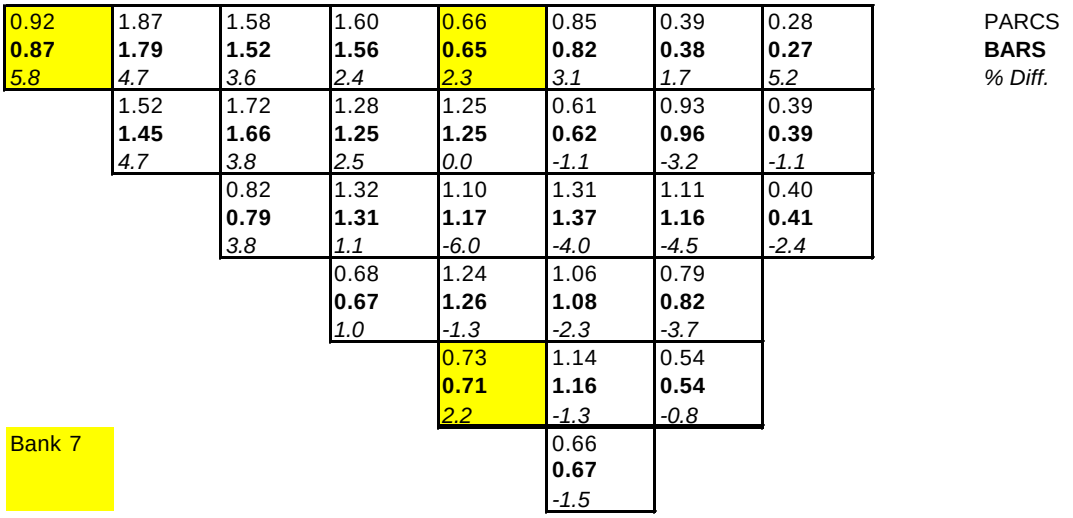

Figure 2.2 Normalized radial power distribution at EOC HZP with banks 5, 6, 7 inserted

Steady-state results for the control rod worths at BOC, HZP are shown in Table 2.3 with comparisons to calculations done by Russian colleagues at RRC-KI using the coupled BARS/RELAP5 code [10]. As seen in Table 2.3, the PARCS predictions for rod worths at BOC were again found to be less than those computed by BARS/RELAP5, differing from 2 to 12%. The discrepancies were larger for the individual control rods 7A, 7B, and 7C. The normalized radial power distributions at BOC HZP with Banks 5,6, and 7 inserted, as shown in Figure 2.3, do not appear to give any immediate physical explanation for these discrepancies, although it is still considered to be linked to the treatment of the boundary conditions at the reflector. Table 2.4 gives the boron and isothermal temperature coefficients, and the reactivity change in going from zero to full power conditions.

Table 2.3 Steady-State Rod Worth Calculations for TMI-1 at BOC, HZP

TMI-1 PWR BOC HZP			
Rod or Bank	PARCS Stand Alone Rod Worth (pcm)	BARS RELAP-5 Rod Worth (pcm)	Difference (%)
5	1247	1337	-6.7
6	723	761	-5.0
7	999	1026	-2.7
7a	245	276	-11.4
7b	149	166	-10.4
7c	473	519	-8.9

0.93 **0.94** *-1.2*	1.79 **1.83** *-1.9*	1.68 **1.72** *-2.2*	1.58 **1.60** *-1.8*	0.72 **0.72** *-0.3*	0.80 **0.79** *2.1*	0.36 **0.36** *1.1*	0.19 **0.18** *4.7*
	1.58 **1.61** *-1.7*	1.70 **1.73** *-1.7*	1.36 **1.38** *-1.2*	1.21 **1.21** *-0.4*	0.66 **0.67** *-0.8*	0.92 **0.94** *-2.6*	0.28 **0.28** *0.8*
		0.92 **0.92** *-0.6*	1.31 **1.31** *0.4*	1.13 **1.14** *-0.7*	1.24 **1.25** *-1.0*	1.14 **1.16** *-1.7*	0.30 **0.30** *-1.2*
			0.77 **0.76** *2.0*	1.27 **1.24** *2.9*	1.08 **1.05** *2.1*	0.69 **0.69** *0.9*	
				0.86 **0.82** *4.1*	1.32 **1.26** *4.4*	0.45 **0.44** *3.9*	
Bank 7					0.64 **0.62** *3.2*		

PARCS
BARS
% Diff.

Figure 2.3 Normalized radial power distribution at BOC HZP with banks 5, 6, 7 inserted

Table 2.4 Reactivity Coefficients for TMI-1 PWR at BOC

Boron Coefficient (pcm/ppm)	-6.26
Isothermal Temperature Coefficient (pcm/C)	-8.00
Power Defect at Hot Full Power (pcm)	-1251

3. DISCUSSION OF RESULTS

3.1 Transient Runs at EOC and BOC

Transient simulations were performed with PARCS to evaluate the TMI-1 core neutronics and thermal-hydraulics behavior in the event of a prompt-critical REA from HZP at both EOC and BOC. The control rod 7A was ejected in 100 ms at a constant rate. The PARCS simulation modeled a reactor trip when the power level reached 112% of the normal full power level (2772 MWth). Shutdown banks 1 to 4 begin insertion 400 ms after the setpoint is reached, and are fully inserted in 2.2 s moving at a constant rate.

Power during the REA transients for both EOC and BOC are shown in Figures 3.1 to 3.3 with different scales being used on each graph. The corresponding reactivity traces are given in Figure 3.4. The ejected rod worths in the EOC and BOC cases are $1.22 and $1.19, respectively. Initially the negative feedback from the moderator and Doppler components due to the rising moderator and fuel temperature is negligible; therefore, the control rod worth is approximately the same as the total reactivity. Control rod 7A is fully withdrawn in 100 ms, and the peak reactivity is reached shortly thereafter as can be seen in Figure 3.4

After rod 7A is fully withdrawn, negative feedback from fuel (primary) and moderator (secondary) begins to reduce the total reactivity and limit the maximum power level. Negative feedback increases until the reactivity drops below prompt critical, and the power begins to decline. The BOC case reaches a peak power of 936% at 268 ms while the EOC case reaches a peak power of 387% at 344 ms. The pulse width in the BOC case is 43.5 ms and for the EOC case the pulse width is 63.0 ms. The BOC transient reaches 112% power at 230 ms, trips at 630 ms, and has all control rod banks fully inserted by 2.8 s. The slower EOC transient reaches 112% power at 300 ms, trips at 700 ms, and has all control rods inserted by 2.9 s.

Figures 3.5 and 3.6 provide the core maximum values for local (defined for each mesh block) fuel temperature and enthalpy. The fuel in the BOC REA reaches a maximum pellet temperature and enthalpy of 574°C and 36.7 cal/g at 0.685 s, equivalent to a 19.8 cal/g maximum enthalpy increase. The fuel in the EOC REA reaches a maximum pellet temperature and enthalpy of 497°C and 31.4 cal/g at 0.722 s, equivalent to a 14.5-cal/g maximum enthalpy increase. The differences in the results between the BOC and EOC cases with comparable rod worths can be explained by the higher burn-up in all the assemblies at EOC. There is more fissile material in the core at BOC than at EOC; hence, the fission reaction rate and power induced by a given rod ejection of equal worth will be higher at BOC than at EOC.

The total reactivity drops off more quickly in the EOC case after the shutdown control rods are inserted from the top of the core (see Figure 3.4) because the neutron flux and power are peaked more towards the top of the core than in the BOC case. The flux and power is peaked towards the top of the core at EOC (see Figure 3.7) because there is a higher burn-up of fissile fuel near the bottom of the core. The higher burn-up near the bottom of the core is caused by the lower coolant temperature and higher moderator density which increase the localized fission reaction rate.

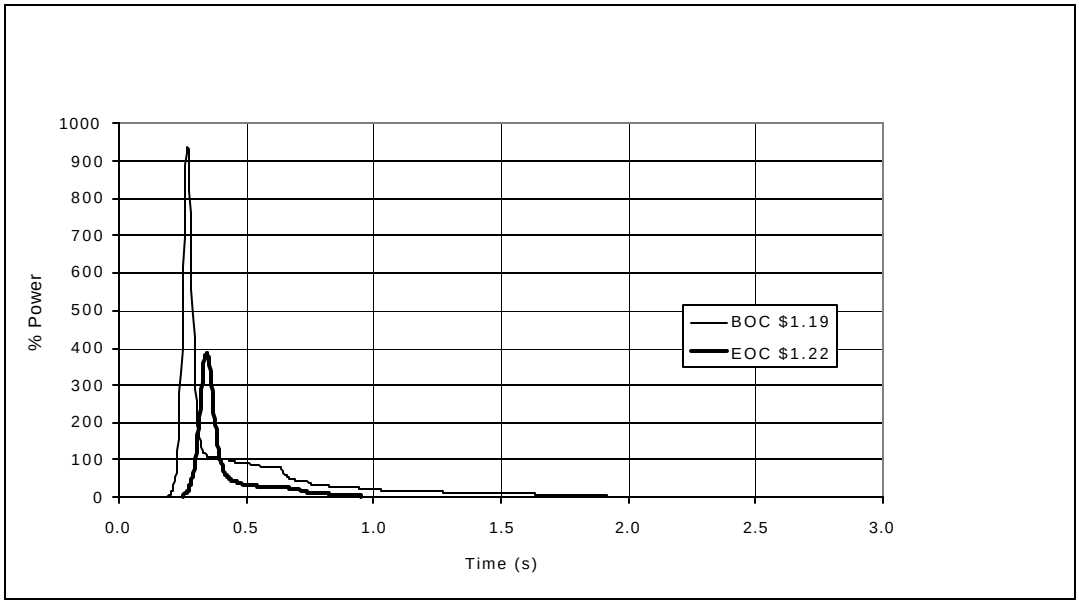

Figure 3.1 Power transients for REA from HZP

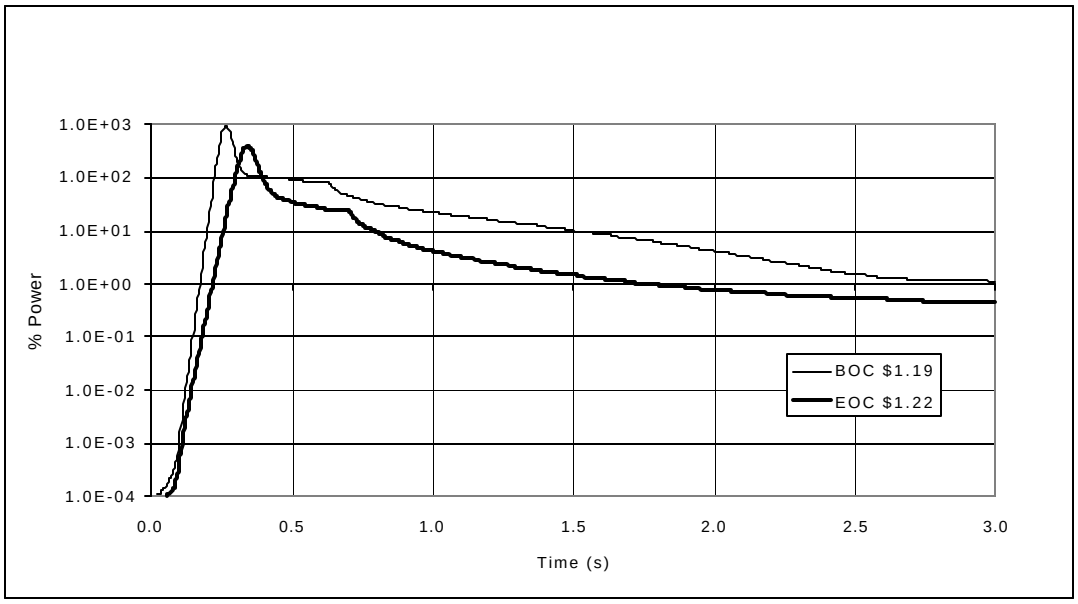

Figure 3.2 Power transients for REA from HZP

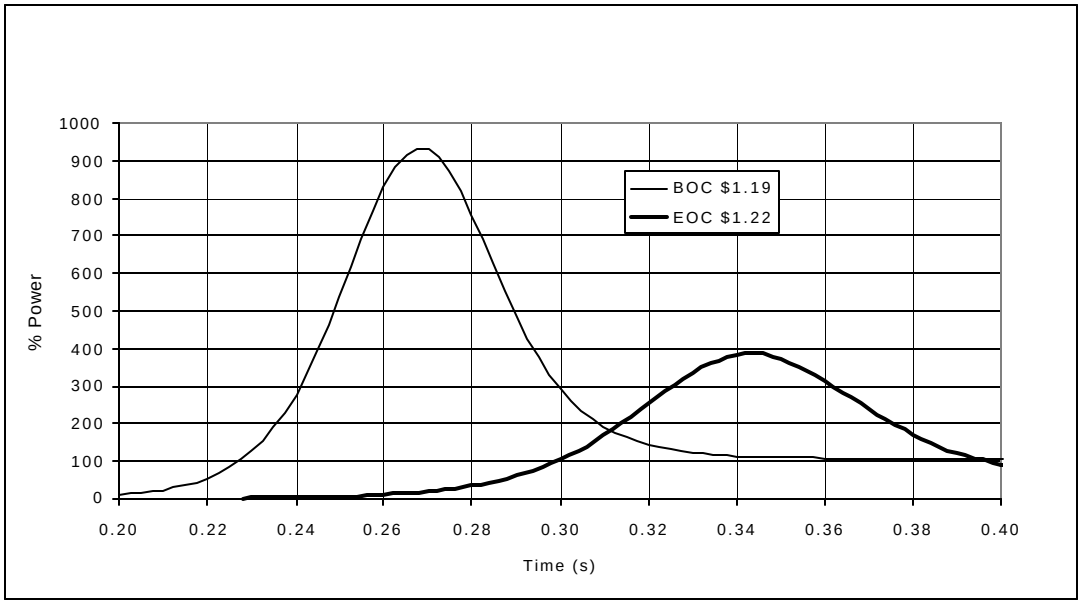

Figure 3.3 Power transients for REA from HZP

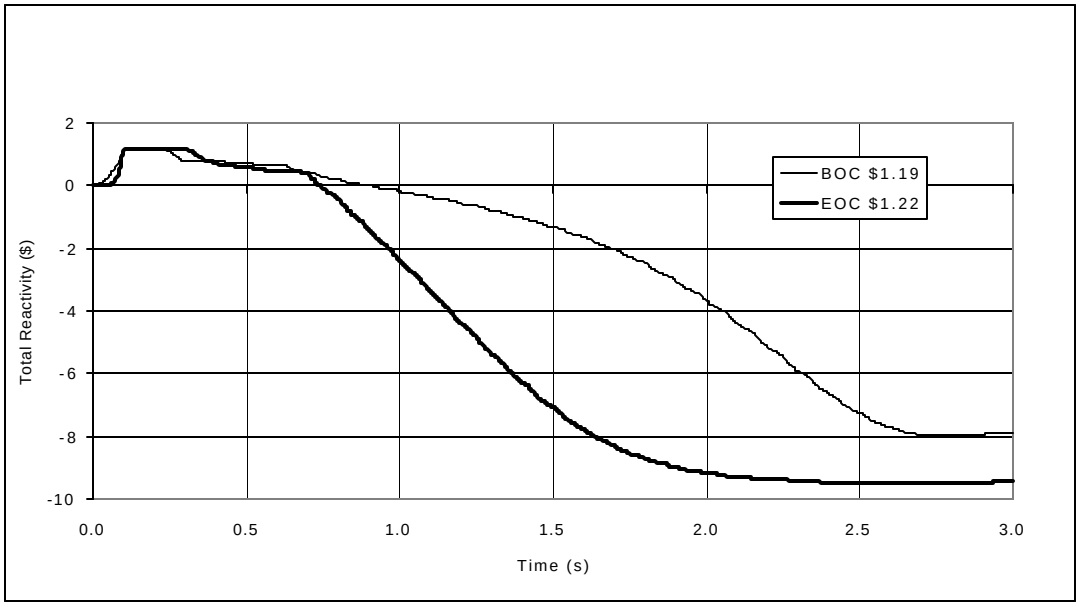

Figure 3.4 Reactivity transients for REA from HZP

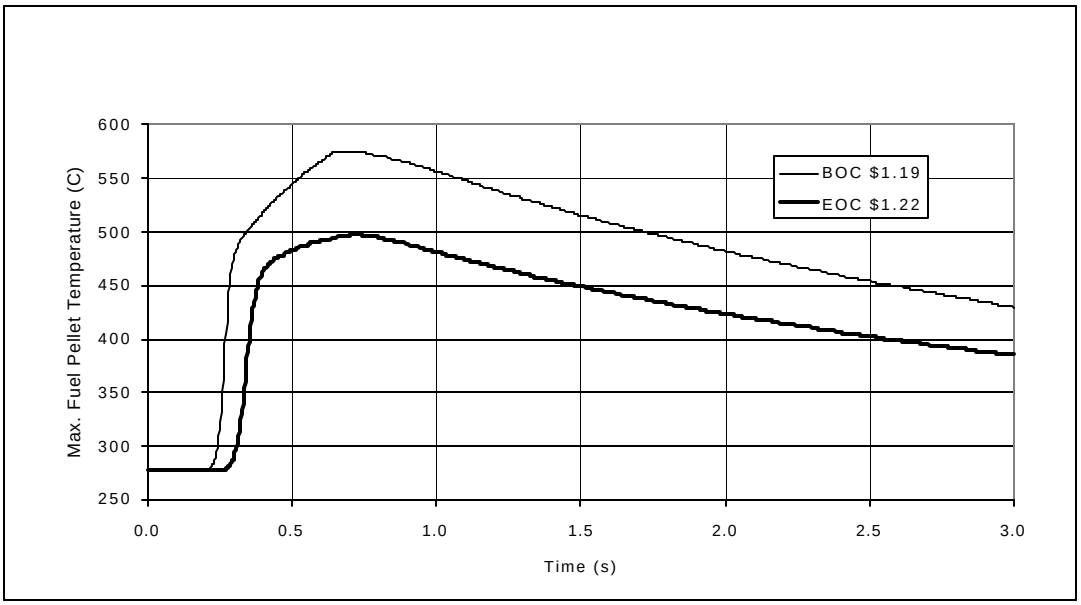

Figure 3.5 Maximum fuel pellet temperature transients for REA from HZP

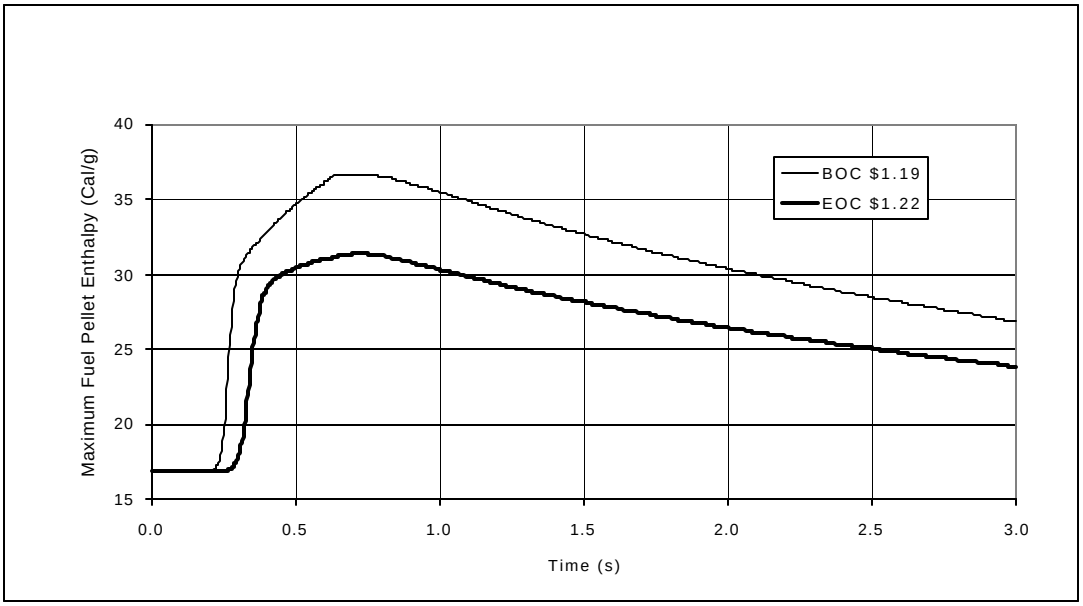

Figure 3.6 Maximum fuel pellet enthalpy for REA from HZP

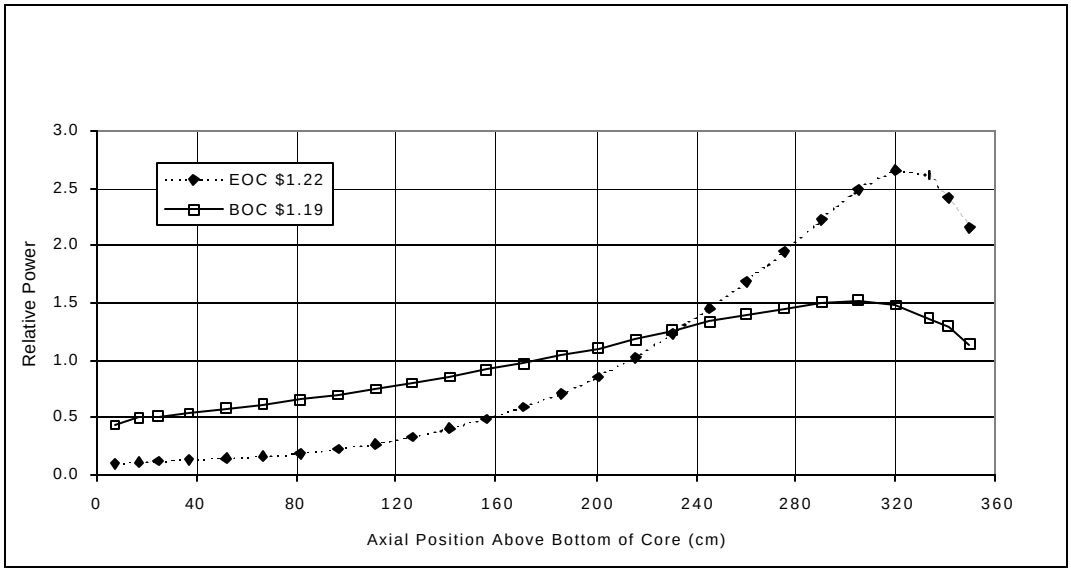

Figure 3.7 Initial normalized axial power distribution at HZP

3.2 Parametric Studies of Rod Worth and Delayed Neutron Fraction

A set of parametric studies were completed in which the multiplication factors on the macroscopic absorption and fission yield cross sections were adjusted to artificially change the worth of control rod 7A in the central fuel assembly. In addition to variation of rod worth, the delayed neutron fraction at EOC was varied from 70 to 120% of the nominal value. For each transient simulation of a given rod worth and delayed neutron fraction, there would be an associated pulse width and maximum increase in fuel pellet enthalpy.

The variation of the maximum enthalpy rise with rod worth normalized by the delayed neutron fraction (i.e., in units of dollars), is given in Figure 3.8. The dependence of fuel enthalpy with rod worth is approximately linear, and it increases with the delayed neutron fraction. As the value of the delayed neutron fraction at EOC approaches that at BOC, so too does the enthalpy rise. For example, the enthalpy rise for a $1.5 REA is approximately 26 cal/g for EOC (â = 0.005211), 34 cal/g for EOC with 120% â (0.006253), and 37 cal/g for BOC (â = 0.006323). For REAs with rod worths below $1.5, the enthalpy rise is less than 40 cal/g. To get an enthalpy rise above 100 cal/g requires an REA of more than $2.3 for the conditions assumed in these studies.

The variation of the maximum enthalpy as a function of the difference between the rod worth and the delayed neutron fraction is given in Figure 3.9. All the data points at EOC for various rod worths and delayed neutron fractions collapse onto a single (almost) linear curve. Hence, the absolute difference between the ejected rod worth and the delayed neutron fraction, the absolute reactivity above prompt critical, determines the maximum fuel pellet enthalpy rise, with all other quantities fixed. The curve for the BOC case is set about 5 to 10 cal/g higher than most of the curves for EOC at any given rod worth exceeding the delayed neutron fraction. As noted previously, the higher enthalpy rise for the BOC case can be explained by the presence of lower burn-up assemblies at BOC. Lower burn-up assemblies will experience a higher fission rate and power increase for a given rod worth during an REA.

A plot of the locus of points for a fixed maximum fuel pellet enthalpy increase as a function of the delayed neutron fraction and the rod worth in dollars above prompt critical, is shown in Figure 3.10. This result is consistent with the linear relationships shown in Figures 3.8 and 3.9.

The variation of the full-width-at-half-maximum (FWHM) power pulse widths for various REA events at EOC and BOC are shown in Figures 3.11 to 3.13. The FWHM is based on total reactor power but is the same for the power in individual assemblies. According to Figure 3.11, the pulse width tends to have an inverse relationship with the normalized rod worth, and goes down with increasing delayed neutron fraction. The pulse width is even lower at BOC than at EOC for a given rod worth. According to Figure 3.12, all the data points at EOC for various rod worths and delayed neutron fractions collapse onto a single curve when the pulse width is plotted against the absolute difference between the rod worth and the delayed neutron fraction. The pulse width has an inverse relationship with the reactivity in excess of prompt critical. Since the maximum fuel pellet enthalpy rise is proportional to the absolute reactivity, it is no surprise that the pulse width also tends to be inversely proportional to the fuel enthalpy rise (Figure 3.13). The pulse width for a given enthalpy rise tends to be slightly lower at BOC than at EOC. For an enthalpy rise of more than 40 cal/g, the FWHM pulse width is less than 20 ms.

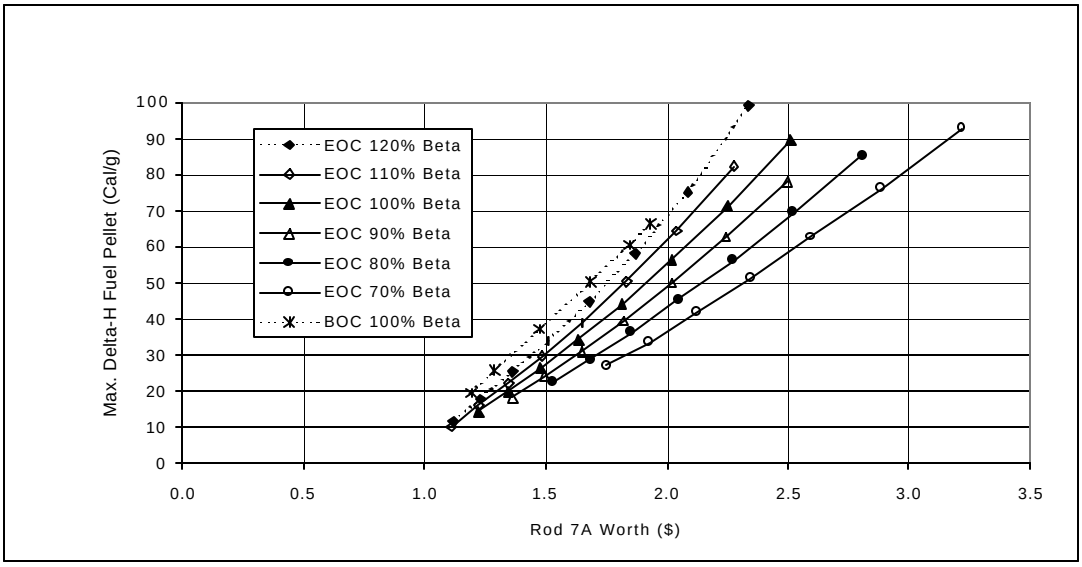

Figure 3.8 Maximum rise in fuel pellet enthalpy for REA from HZP

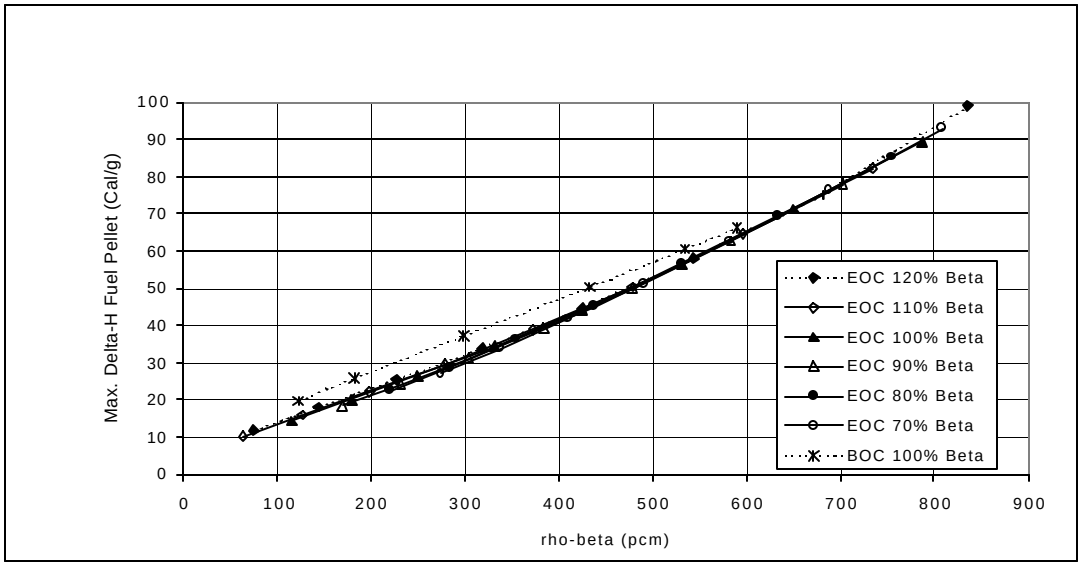

Figure 3.9 Maximum rise in fuel pellet enthalpy for REA from HZP

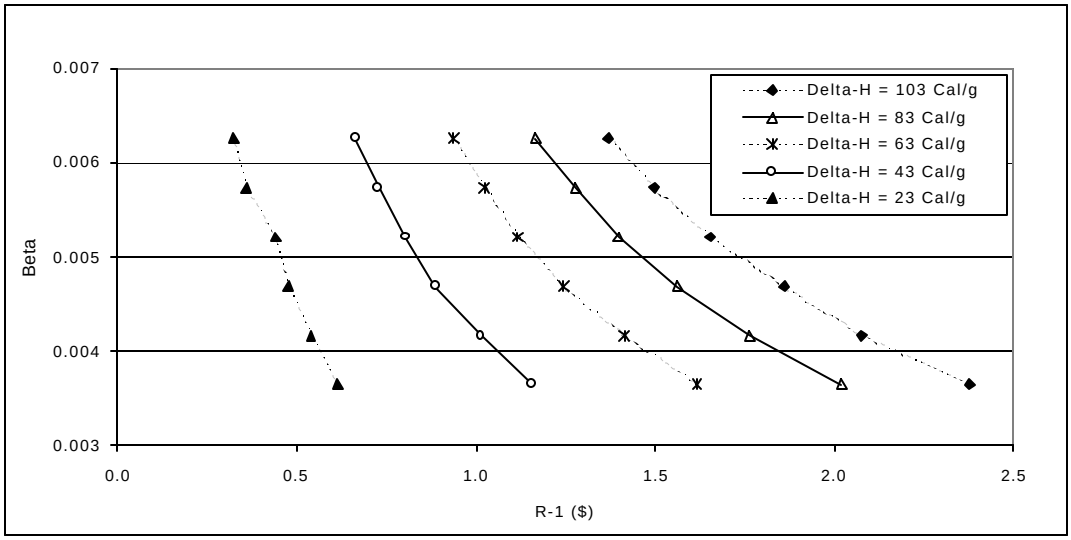

Figure 3.10 Locus of beta and rod worth for fixed maximum rise in fuel pellet enthalpy

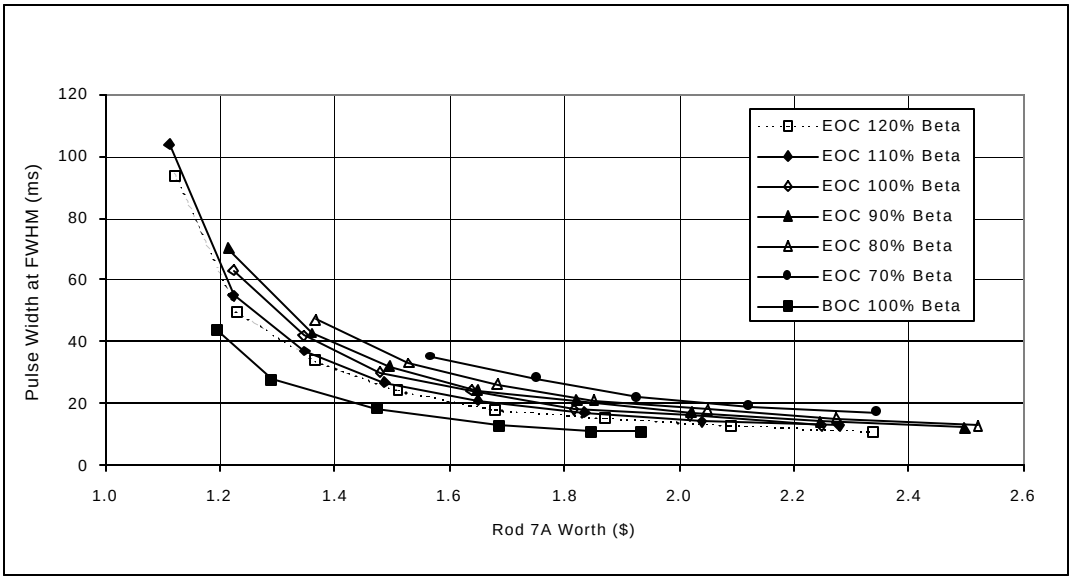

Figure 3.11 Pulse width at FWHM for REA from HZP

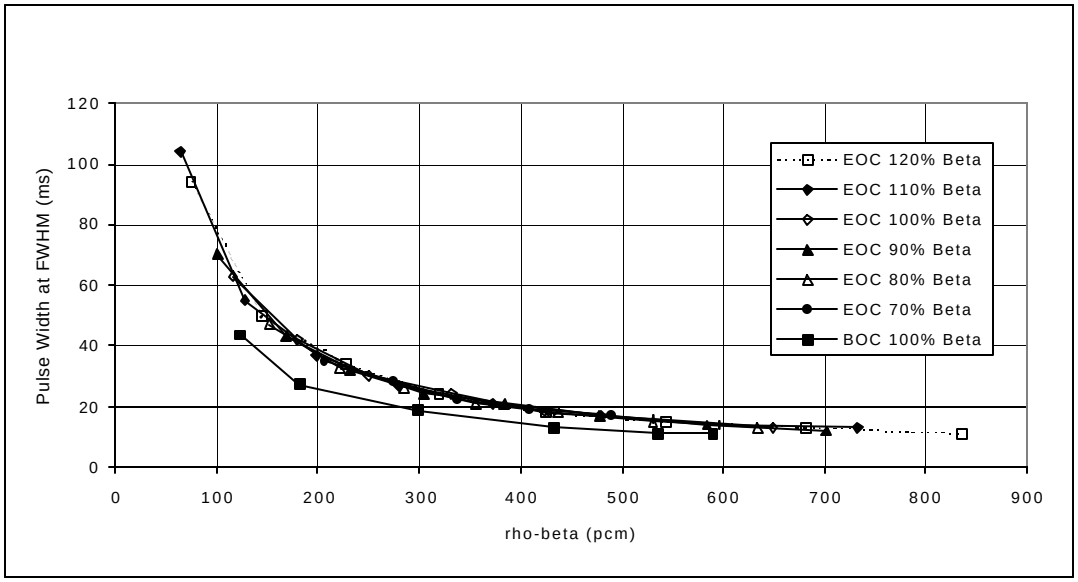

Figure 3.12 Pulse width at FWHM for REA from HZP

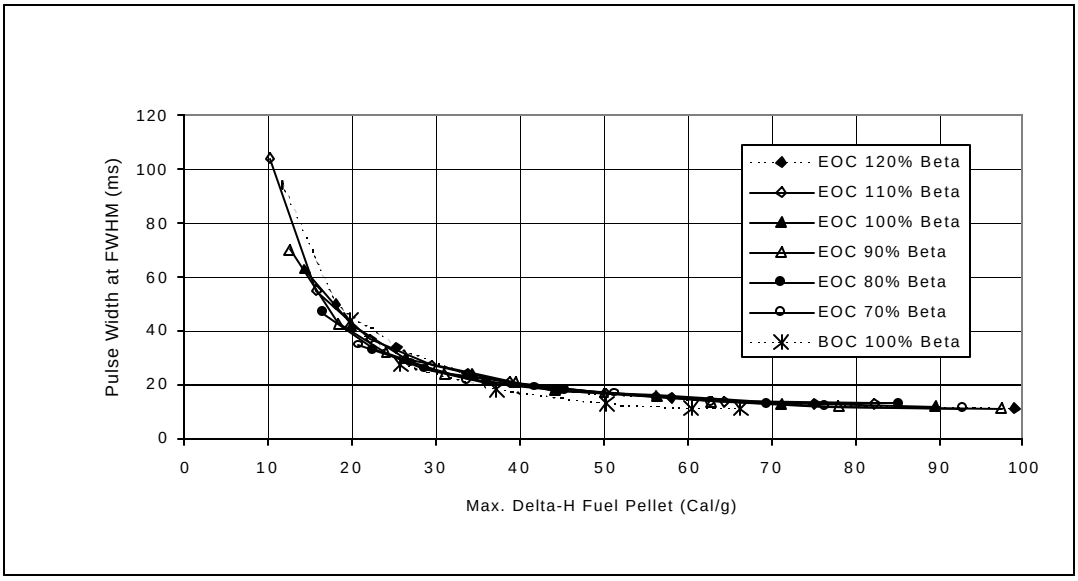

Figure 3.13 Pulse width at FWHM for REA from HZP

3.3 Comparison with Nordheim-Fuchs Model

The Nordheim-Fuchs zero-dimensional adiabatic model [11] gives an analytical estimate of the energy release that occurs during a super-prompt-critical power excursion. It is based on the point-kinetics model and applicable to a step insertion of reactivity and a linear negative temperature feedback on the reactivity. Although it is a very simple model, it is useful to consider because it has been shown in the past to be capable of improving our understanding of the REA [3, 6]

According to the Nordheim-Fuchs model, the maximum specific power during the super-prompt-critical transient which is terminated by temperature feedback is given by:

$$P_{\max} = \frac{\left(r_0 - b\right)^2 c_p}{2\, a\, \ell} \tag{3.1}$$

The parameters $\tilde{n}_o$, â, c_p, á, and *l* are the step reactivity change, the delayed neutron fraction, the fuel heat capacity, the absolute value of the negative reactivity temperature coefficient, and the neutron lifetime respectively.

The specific energy deposition in the fuel during the pulse is given by:

$$E = \frac{2\left(r_0 - b\right) c_p}{a} \tag{3.2}$$

The pulse width at FWHM is given by either of the following

$$t = \frac{3.535\, \ell}{\left(r_0 - b\right)} \tag{3.3}$$

(3.4)

$$t = \frac{7.07\, \ell\, c_p}{a\, E}$$

These relationships are approximately valid when discussing the REA. As can be seen in Figure 3.9 the energy deposited (the increase in fuel enthalpy) is indeed proportional to (ñ-â) as specified by Equation 3.2). Note that this relationship is valid even though Figure 3.9 is a plot of the energy deposition at a particular location in the core rather than the total energy deposition as specified in Equation 3.2. Note too that the

simplistic model is approximately valid in spite of the fact that the power pulse in an REA is not completely terminated, i.e., the power has a tail which adds to the energy deposited during the initial pulse.

The previous results for pulse width shown in Figures 3.12 and 3.13 also fit with the simple model and Equations 3.3 and 3.4, respectively. Note again that these relationships are valid in spite of the fact that the energy deposition plotted is a local rather than global quantity. The global parameters in the simple model (c_p, á, and *l*) will vary from one reactor core composition and design to the next. Because these parameters at BOC differ from those at EOC, the constants of proportionality relating the pulse width to the energy deposition, and reactivity will change as well.

3.4 Effect of Ejected Rod Location

The variation of the maximum fuel pellet enthalpy increase with control rod worth for an REA at EOC, HZP for different control rods is shown in Figure 3.14. The three control rods 7A, 7B, and 7C are located as shown in Figure 2.1 Each location has a different control pattern surrounding it and different fuel assemblies and burnups. Nevertheless, the results in Figure 3.14 show that the location of the ejected rod does not appear to matter as much as the worth of the rod itself. Naturally, in an actual core, the worth of the ejected rod will depend on the location.

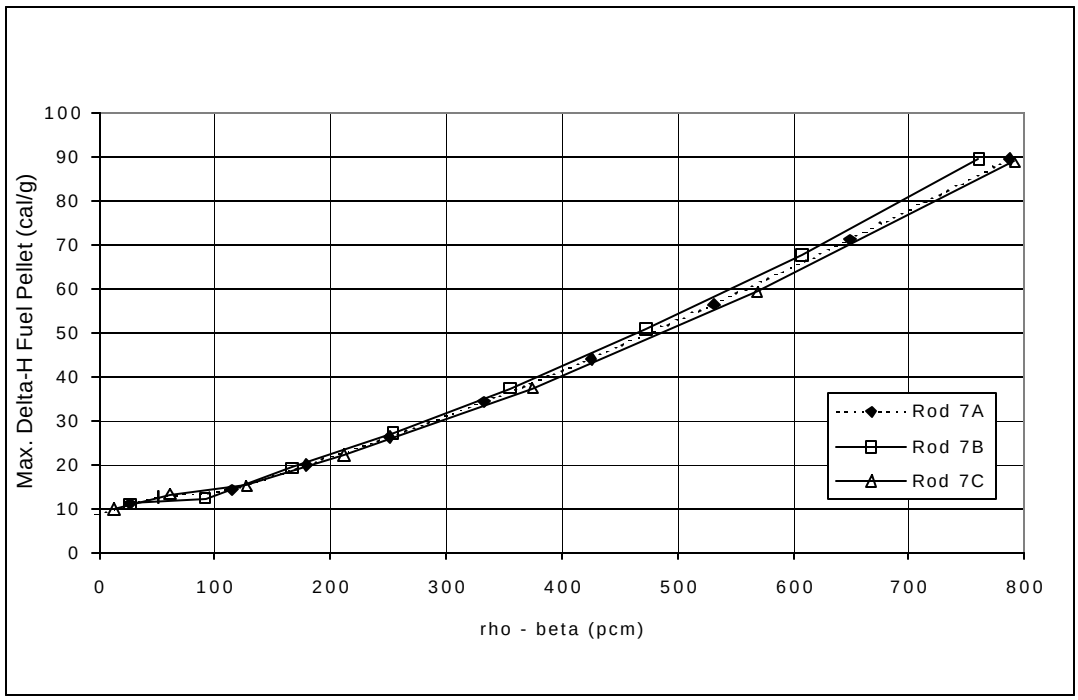

Figure 3.14 Maximum enthalpy rise variation with rod worth for different control rods during REA

3.5 Effect of Reactor Trip

The effect of having no trip of the reactor in the first three seconds of an REA at EOC, HZP is shown in Figures 3.15 to 3.17. The total reactor power typically exceeds the trip value (112%) at approximately 0.3 s, so scram does not begin until about 0.7 s. Since the pulse width for the REA is smaller (usually much less than 100 ms) than the delay time (400 ms), and the drop time (2200 ms) for the shutdown banks, most of the energy deposition in the fuel pellet occurs well before the beginning of reactor scram. Figure 3.15 shows when the reactivity changes due to control bank insertion and Figure 3.16 shows the effect on power. The resulting change in maximum fuel enthalpy (defined for the no-trip case at 3 s) is only ~2 cal/g for a $1.2 rod worth as can be seen on Figure 3.17. The differences are smaller when the rod worth increases. The peak fuel centerline temperature increases between 100 and 200°C due to the failure of the reactor to scram.

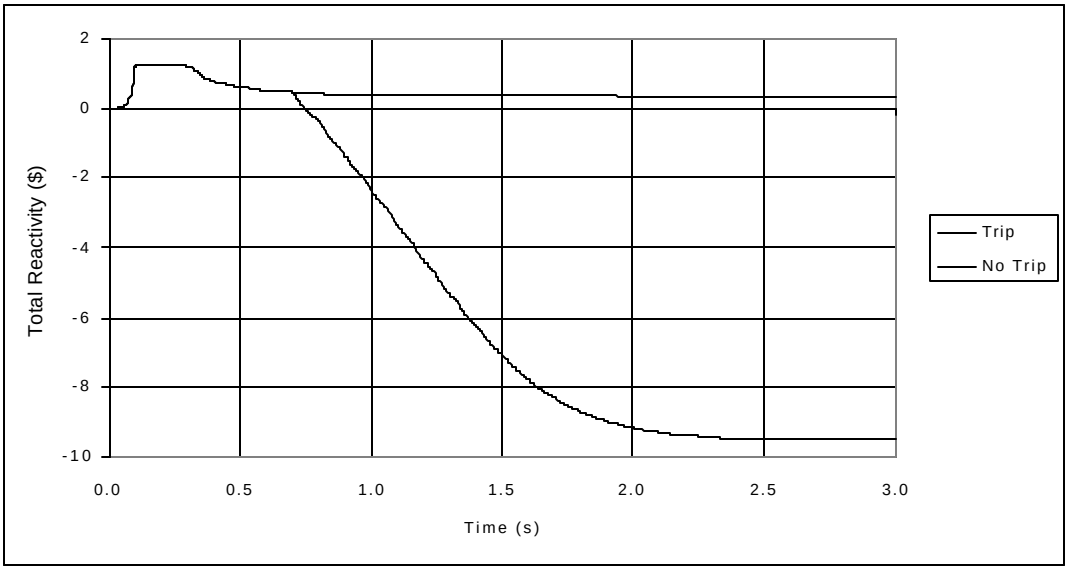

Figure 3.15 Effect of trip on total reactivity in REA at EOC HZP

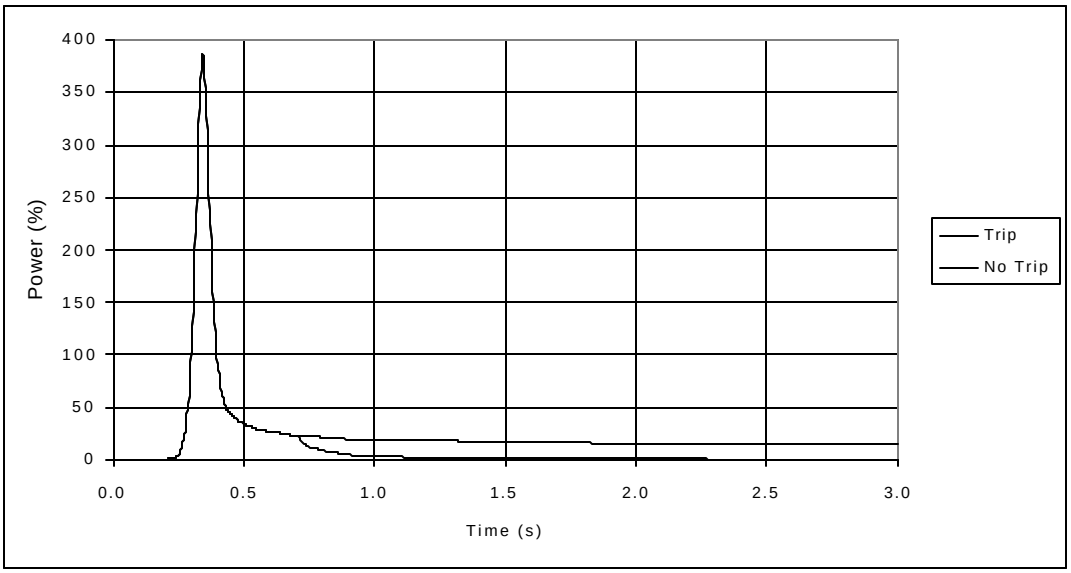

Figure 3.16 Effect of trip on power in REA at EOC HZP

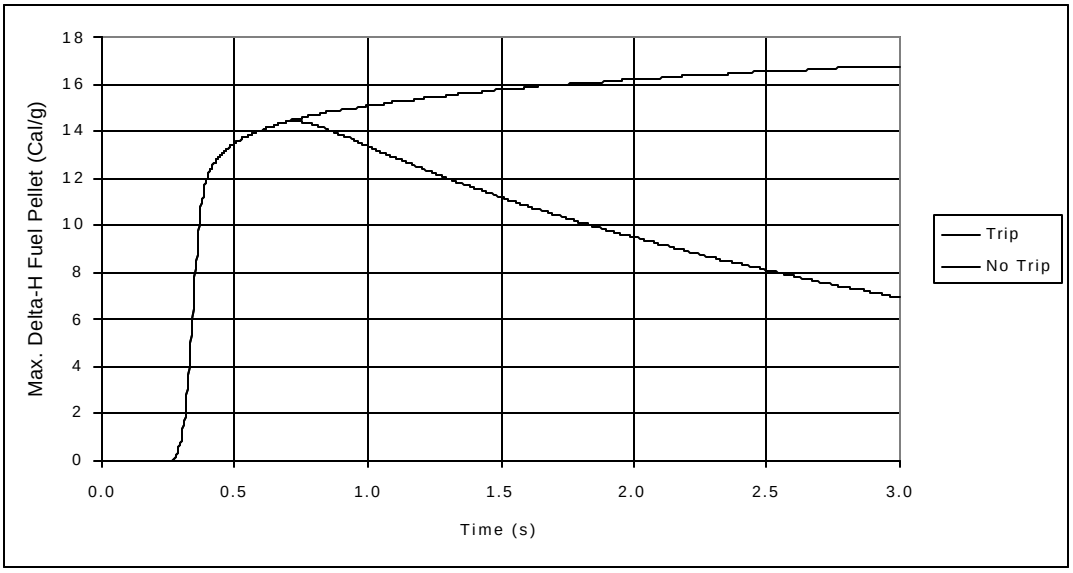

Figure 3.17 Effect of trip on max. fuel pellet enthalpy rise in REA at EOC HZP

3.6 Effect of Gap Conductance

The effect of gap conductance on the maximum fuel pellet temperature and enthalpy rise is shown in Figures 3.18 and 3.19. As the gap conductance is increased, heat transfer to the coolant improves, and the peak fuel pellet temperature goes down, but the effect is not particularly significant. When the gap conductance is changed by 20%, the maximum fuel pellet temperature changes by less than a few degrees, and the maximum fuel pellet enthalpy rise changes by less than 1 cal/g.

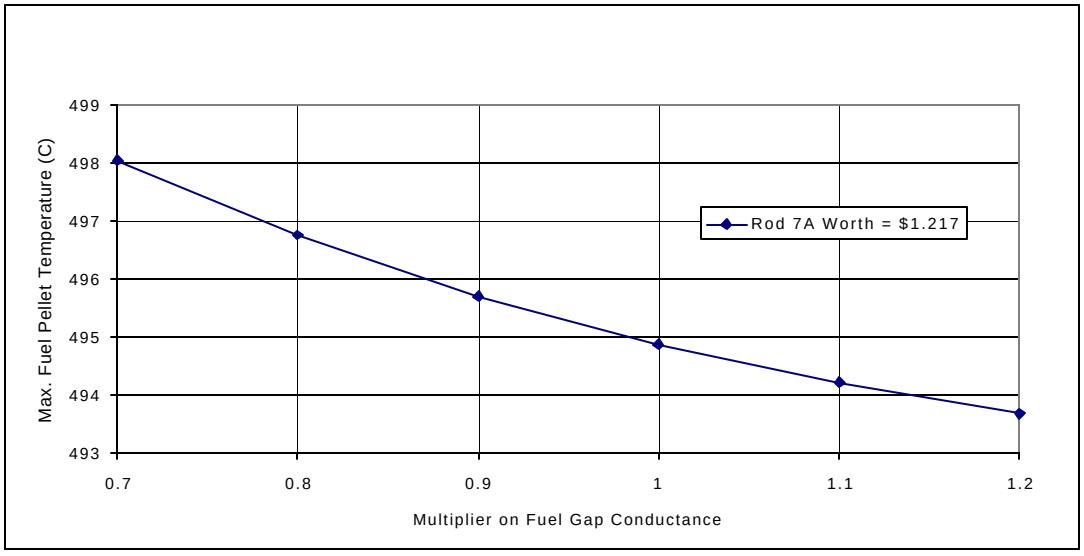

Figure 3.18 Effect of gap conductance on maximum fuel pellet temperature in an REA at EOC HZP

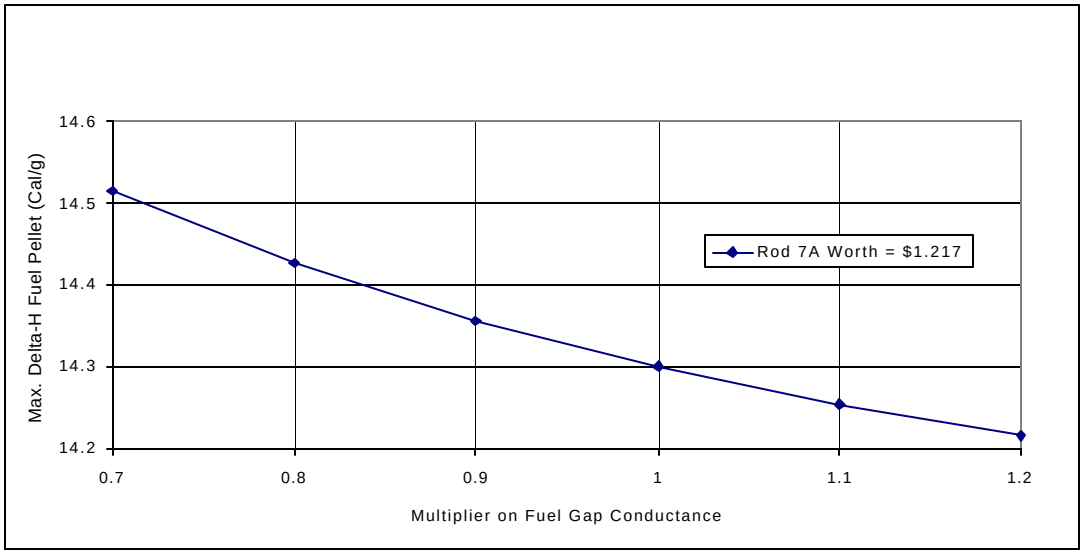

Figure 3.19 Effect of gap conductance on maximum fuel pellet enthalpy rise in an REA at EOC HZP

3.7 Effect of Fuel Heat Capacity

The effect of fuel heat capacity on the peak fuel centerline temperature and the maximum increase in fuel pellet enthalpy is shown in Figures 3.20 and 3.21. The maximum fuel centerline temperature has a weak decreasing linear dependence on the heat capacity. When the fuel heat capacity is increased by 20%, the maximum fuel centerline temperature decreases by approximately 10°C. For a given energy deposition, fuel with a higher heat capacity will have a lower temperature.

The maximum fuel pellet enthalpy rise has a linear relationship with the fuel heat capacity. Although temperature may go down slightly as c_p increases, since enthalpy is proportional to c_p and temperature, it increases with an increase in c_p. The sensitivity $(dh_f/h_f)/(dc_p/c_p)$ is approximately unity. This result is consistent with that suggested earlier by the Nordheim-Fuchs model which showed (Eq. 3.2) that the energy deposition is directly proportional to the fuel heat capacity. Thus, for example, if the fuel heat capacity increases by 20%, the maximum fuel pellet enthalpy rise should increase by 20%.

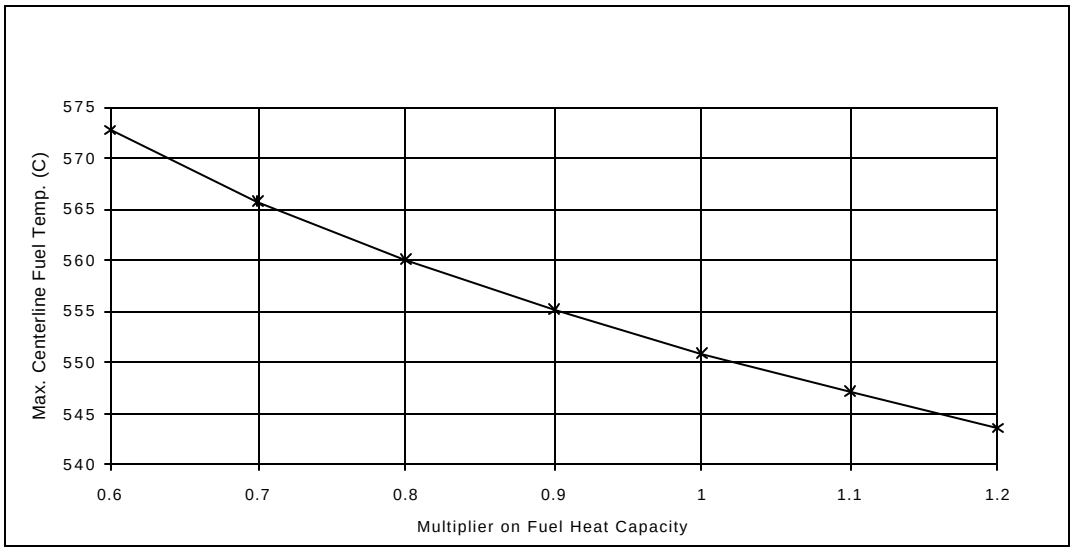

Figure 3.20 Effect of fuel heat capacity on maximum centerline temperature in REA at EOC HZP

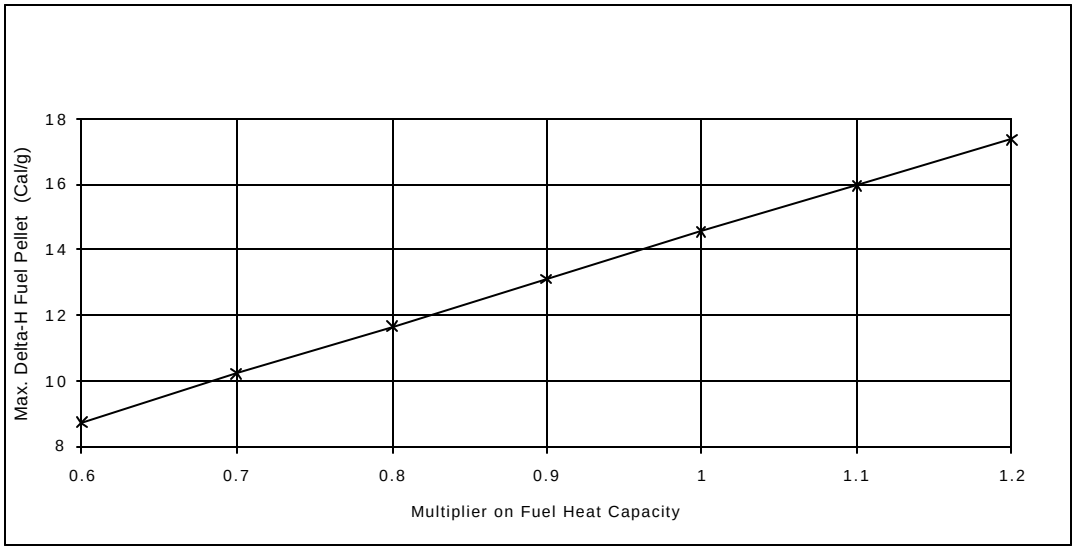

Figure 3.21 Effect of fuel heat capacity on maximum fuel pellet enthalpy rise in REA at EOC HZP

3.8 Effect of Fuel Pellet Power Distribution

In the PARCS heat conduction model, the power density (W/cm^3) within a fuel rod is assumed to be uniform for all fuel rods modeled in the core. This is a common assumption although it is well-known that the power density is peaked toward the outside of the pellet and that this peaking becomes more accentuated with burnup (the so-called rim effect). This is the result of both the depression of the thermal neutron flux within the fuel pellet [12] and the variation of fissile isotopes within the fuel pellet. The latter shifts over the fuel cycle due to non-uniform burn-up of fuel and the conversion of U-238 into various isotopes of plutonium preferentially at the edge of the pellet. Previous calculations and experimental data [13, 14] demonstrate that the power distribution rises sharply near the edge of the fuel pellet, as shown in Figure 3.22.

The effect of a non-uniform power distribution on the REA analysis can be tested. However, since the existing version of the PARCS code is programmed only to calculate the fuel temperature on the basis of a uniform power density, the coupled PARCS/RELAP5 code must be used instead. To model the power distribution in the fuel pellet, 20 mesh points are used instead of the usual 6 and calculations were done using a uniform and non-uniform mesh (see Figure 3.22).

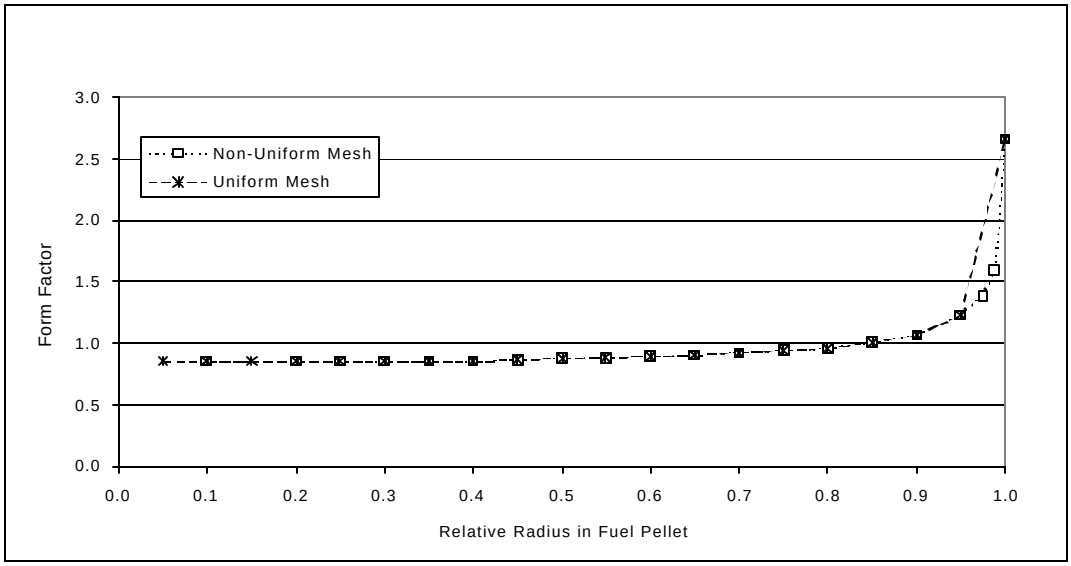

Figure 3.22 Sample fuel pellet radial power distribution in several LWR fuel types [13]

The effect of a non-uniform power distribution in the fuel pellet is shown in Table 3.1. Two base case calculations were done with a uniform power distribution. One was done with the PARCS code, and the other was done with the coupled PARCS/RELAP5 code. Two calculations were done with the non-uniform power distribution, one using a uniform spatial mesh for the temperature distribution calculation, the other using a non-uniform spatial mesh. As seen in Table 3.1, there are slight differences between the PARCS and PARCS/RELAP5 results. The PARCS/RELAP5 code gives a higher peak power and a shorter pulse width, but the peak centerline and fuel pellet temperatures differ from those computed by PARCS by less than 6°C. When a power distribution peaked as in Figure 3.22 is used, both the peak centerline and fuel pellet temperatures in an REA drop between 50 and 120°C. The peak fuel pellet enthalpy increase also drops 3-5 cal/g. The use of a non-uniform spatial mesh for the temperature calculation results in less of a drop in the fuel temperatures and enthalpy than with a uniform mesh.

The drop in enthalpy is due to the additional conduction of heat out of the pellet due to the larger temperature gradient at the surface as a result of the power peaking at the surface. Since a uniform power distribution gives a higher maximum fuel pellet temperature and enthalpy rise during a transient calculation of an REA than a non-uniform power distribution, the calculations that have been performed using a uniform fuel pellet power distribution can be considered to be more conservative. However, if departure-from-nucleate-boiling rather than fuel enthalpy was the criterion of interest, then the additional heat transfer to the clad and then the water that occurs when a non-uniform power distribution is used would help make the calculation more conservative. Since both are actually of concern, it is of interest to try to do the heat transfer calculation as rigorously as possible.

Table 3.1 Comparison of Effect of Power Distribution in Fuel Pellet in TMI-1 PWR REA

Code	PARCS	PARCS RELAP5	PARCS RELAP5	PARCS RELAP5
Fuel Power Shape	Uniform	Uniform	Non-Uniform	Non-Uniform
Fuel Mesh	Uniform	Uniform	Uniform	Non-Uniform
Rod 7A Worth,$	1.218	1.221	1.221	1.221
Initial Fuel Temperature (°C)	278	278	278	278
Max. Centerline Temperature (°C)	569	570	452	485
Max. Fuel Pellet Temperature (°C)	513	518	444	468
Max. Delta-H Fuel Pellet (Cal/g)	15.6	15.9	10.8	12.4
Peak Power (%)	402	463	302	353
Pulse Width (FWHM) (ms)	66	61	67	65

3.9 Effect of Core Power Level

In the calculations discussed above, the REA is initiated from HZP conditions with Banks 5, 6, and 7 fully inserted. Analysis of an REA event at HZP is considered to be the most conservative since the highest worth rods are expected at these conditions and the corresponding fuel enthalpy should be largest relative to initial conditions at higher power. In a PWR, the increase in power level from HZP to hot full power (HFP) is accomplished by the withdrawal of the regulating control banks (Banks 5, 6, and 7). Technical specifications for safe operation of a PWR place limits on the amount of withdrawal for each bank as power is increased. A sample set of rod position limits for a PWR [15] similar to that represented in the PARCS model used for this study is shown in Figure 3.23. The restricted power limit curve is the maximum power that the reactor can be operated at safely for a given total withdrawal of all the regulating control banks. If the reactor power level exceeds this limit, then the reactor is shutdown. Under normal operating conditions, the power should be at a lower level for a given total bank withdrawal, as given by the lower curve in Figure 3.23. For example, if the banks are withdrawn 163% (Bank 5, 100%, Bank 6, 63%, Bank 7, 0%), the maximum power normally permitted is approximately 30% of full power; however, a power increase to 50% will be tolerated before the reactor is shut down.

Figure 3.24 shows the withdrawal limits for separate banks in relation to the total withdrawal limit. There is a 20% withdrawal overlap between each bank. For example, when the control banks have been 100% withdrawn, Bank 5 has been withdrawn 90%, Bank 6 has been 10% withdrawn, and Bank 7 has been 0% withdrawn. When the control banks have been 200% withdrawn, Bank 5 has been 100% withdrawn, Bank 6 has been 90% withdrawn, and Bank 7 has been 10% withdrawn.

In order to study the effect of going to higher power levels on the worth of central control rod 7A, calculations were done separating the effect of Bank 5 withdrawal from the effect of being at higher power level, i.e., with the rod position limits specified in Figure 3.23 ignored. For example, calculations for the Rod 7A worth at 30% power were done with Bank 5 ranging from 0 to 100% withdrawn, and Banks 6 and 7 fully inserted.

The calculation of the worth of an ejected rod for various power levels and regulating control rod positions can be done by using two steady-state calculations, or by using a transient simulation. The change in the reactivity between two steady state conditions (one with a rod fully inserted, one with a rod fully withdrawn) is the rod worth. Alternatively, the maximum total reactivity in a transient REA analysis with a short rod ejection time (less than 100 ms) can be approximated as the control rod worth since the values of the other components such as Doppler fuel or moderator density are initially negligible due to the delayed feedback effect.

Results for steady state and transient rod 7A worth calculations at EOC for various power levels (1.0×10^{-4}%, 15%, 30% of full power) and control bank 5 withdrawal positions (0 to 100%) are shown in Figure 3.25. The worth of Rod 7A was adjusted to be \$1.2 at HZP with all regulating banks inserted and the remaining calculations were done with no other changes to the data set. For the transient calculations, the rod worth was the maximum control reactivity (\$) during the REA with reactor trip. Initially, the Doppler and moderator reactivity feedback components were small; therefore, the control reactivity was approximately the same as the total reactivity.

As shown in Figure 3.25, the worth of rod 7A at HZP decreases monotonically in a non-linear fashion, dropping from approximately \$1.2 with bank 5 fully inserted to approximately \$0.5 with bank 5 fully withdrawn. The steady state and transient results for rod worth at HZP are almost the same.

As the power level is increased, the steady-state rod worth tends to decrease with power, dropping from approximately \$1.2 at HZP to ~\$1.0 at 15% power, and \$0.93 at 30% power with bank 5 fully inserted. Rod worth also decreases monotonically in a non-linear fashion with bank 5 position; however, the steady state rod 7A worth converges to a value of \$0.50 for all power levels with bank 5 fully withdrawn. Since rod worth decreases with power level *and* with a decrease in control rod insertion within the core, it is concluded that HZP should be the most limiting initial condition for the REA.

To quantify this assertion REA calculations were done based on a rod worth for rod 7A of \$1.3 at 30% power. One calculation at 30% power had Bank 5 initially withdrawn and the calculation at HZP with the identical parameters for rod 7A had Bank 5 initially inserted. The increase in fuel enthalpy for the case from 30% power was 34 cal/g and the increase for the case from HZP was 117 cal/g; the latter due to the fact that the rod worth of rod 7A was almost twice as large with bank 5 inserted and at the lower power.

Another phenomenon observed on Figure 3.25 is that at elevated power levels the transient calculation for rod worth does not match the steady-state calculation. For bank 5 withdrawal fractions below 40%, the rod worth obtained from the transient calculation is significantly larger than the steady-state calculation whereas above 40% the differences are small. In addition, the transient rod worth converges to a value of approximately \$1.2 for all power levels with control bank 5 fully inserted. From 40% to 100% bank 5 withdrawal, the rod worth at 15% and 30% power differs by less than \$0.04. To understand these trends of the rod worth with power level, it is necessary to consider the power distributions obtained under these conditions.

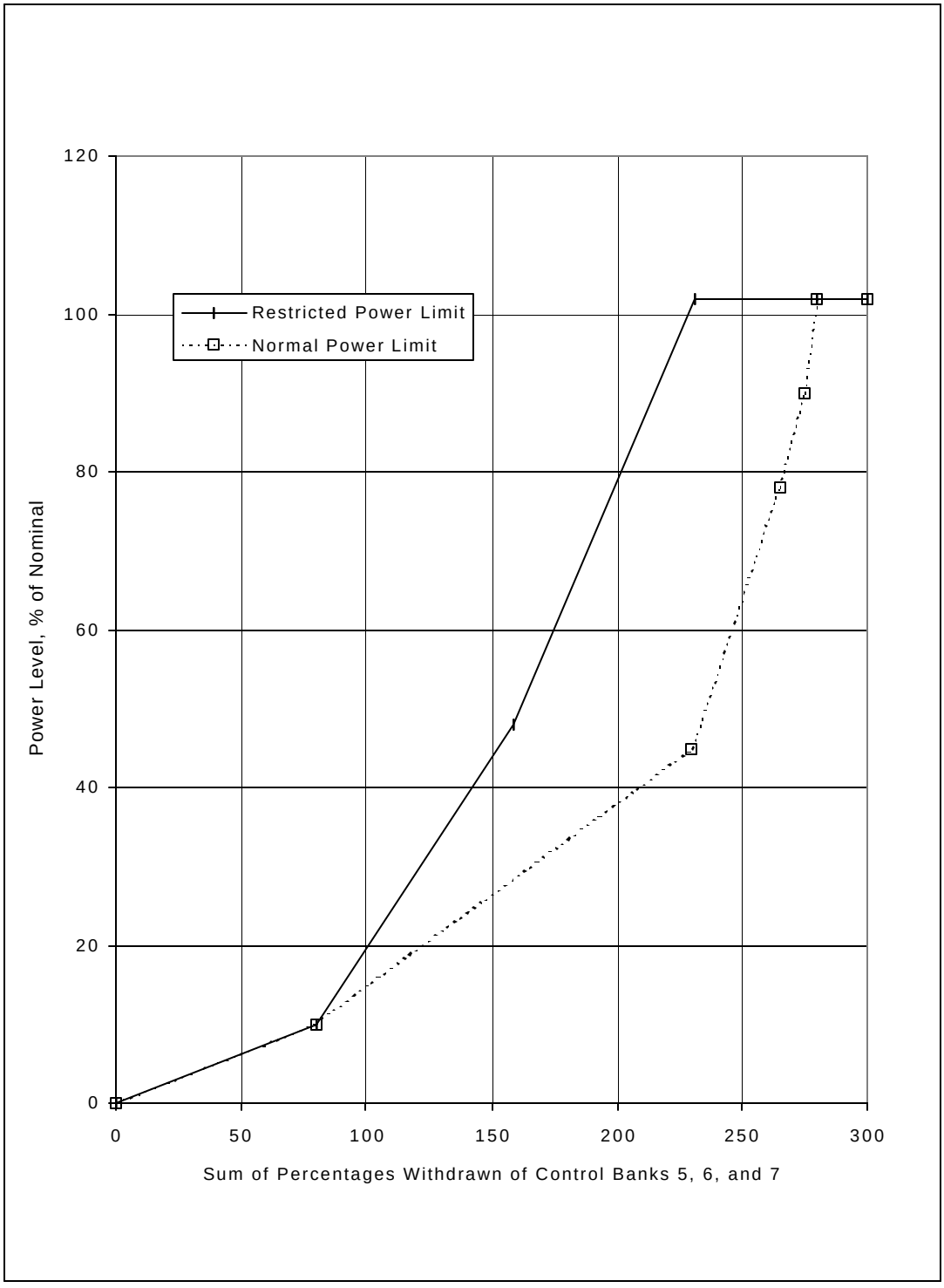

Figure 3.23 Typical rod withdrawal limits in a PWR at various power levels [15]

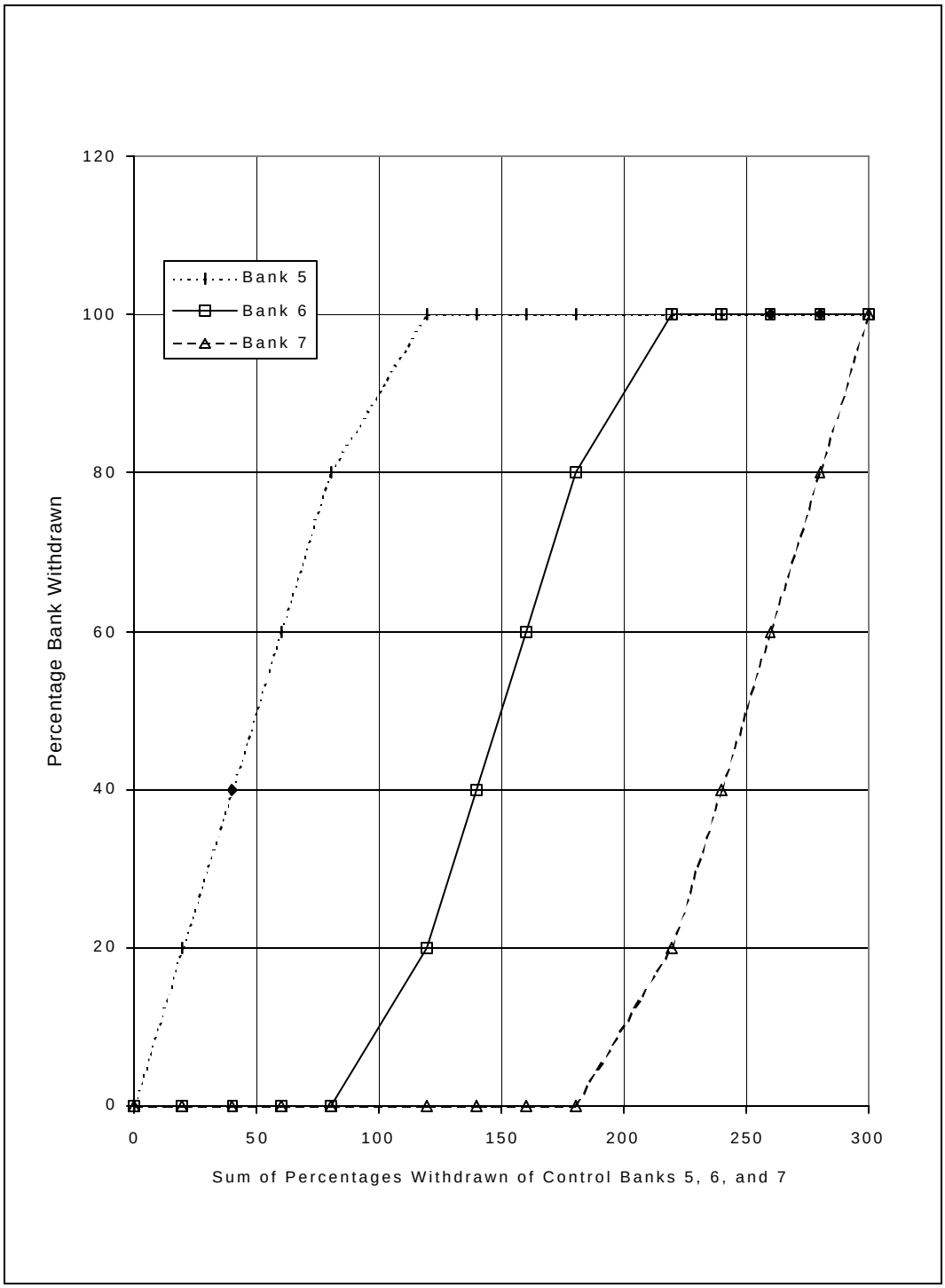

Figure 3.24 Typical individual rod withdrawal limits in a PWR

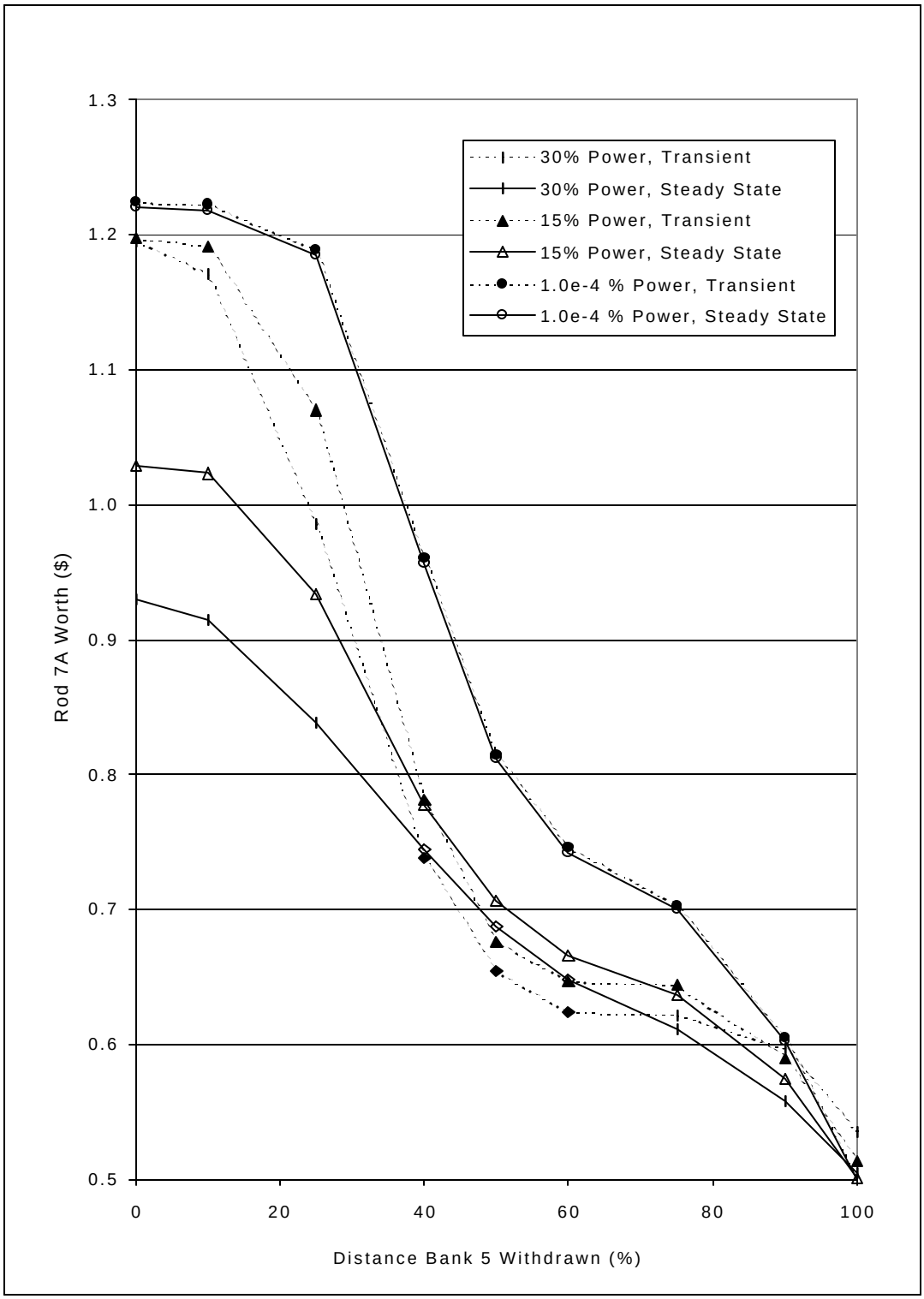

Figure 3.25 TMI-1 PWR EOC control rod 7a worth variation with power level, bank 5 position, and calculation procedure

The steady-state normalized axial power distributions computed by PARCS for EOC at various power levels with control bank 5 fully inserted, and rod 7A fully inserted or withdrawn are shown in Figure 3.26. The relative power is less than unity at core axial positions less than 200 cm above the bottom of the core, and greater than unity at axial positions greater than 216 cm above the bottom of the core. The peak relative power occurs at approximately 320 cm (90%) above the bottom of the 357-cm core height for all power levels. As the power level increases, thermal-hydraulic feedback causes the relative power to decrease in the top part of the core (230 to 357 cm), and increase in the bottom part of the core (0 to 230 cm). There is little difference (usually less than 10%) in the normalized axial power distributions at a given power level for rod 7A inserted or withdrawn.

The steady-state normalized radial (X-Y) power distributions computed by PARCS for EOC at various power levels with control bank 5 fully inserted, and rod 7A fully inserted or withdrawn are shown in Figures 3.27 to 3.29. The radial distributions are shown only for $1/8^{th}$ of the core due to the symmetry. The radial power distributions at all power levels with rod 7A fully inserted are only slightly different. For example, the relative power in the central fuel assembly is 0.228 at HZP, and 0.229 at 30% power. Comparison of all other fuel assemblies show that there is little change in the power distribution with rod 7A fully inserted as the power level is increased from HZP to 30% power. The situation changes when rod 7A is fully withdrawn. The peak normalized power occurs in the in the fuel assembly adjacent to the central assembly, with 7A fully withdrawn, decreasing from 2.68 at HZP to 2.27 at 30% power. As the power level is increased, the radial power distribution becomes flatter, decreasing near the center, and increasing near the radial reflector relative to the HZP case.

In Figure 3.30, normalized radial power distributions are shown for four cases. The steady state power distributions at 30% power with rod 7A fully inserted/withdrawn are shown, as was done in Figure 3.29. In addition, the instantaneous radial power distribution at the maximum control reactivity for the transient calculation starting at 30% power is shown. Finally, the steady state power distribution at HZP with rod 7A fully withdrawn is also shown for comparison. As discussed above, the steady state reactivity worth of rod 7A dropped significantly as the power level was increased from HZP to 30% power while control bank 5 was inserted. However, the transient calculation showed that rod worth at 30% power was approximately the same as that at HZP ($1.2). The fact that the normalized radial power distribution at maximum reactivity for the transient calculation at 30% power is closer to the radial power distribution at HZP than the steady state calculation at 30% power with 7A fully withdrawn is consistent with the observation of the similarity between the transient calculation of the rod worth at 30% power and the rod worth calculation at HZP with control bank 5 fully inserted. For example, in the central fuel assembly, the relative powers at 30% power steady state, 30% power transient, and HZP steady state are 1.77, 2.04, and 2.10, respectively. The first two values differ by 15%, while the latter two differ by only 3%.

In Figure 3.31 the normalized axial power distributions are shown for three of the four cases in Figure 3.30. For the case initially at 30% power, the transient calculation of the power distribution changes little from the steady state calculation with rod 7A removed but differs significantly from the HZP case. Hence, the key difference between the transient and steady state calculations of rod worths is linked to the normalized radial power distributions.

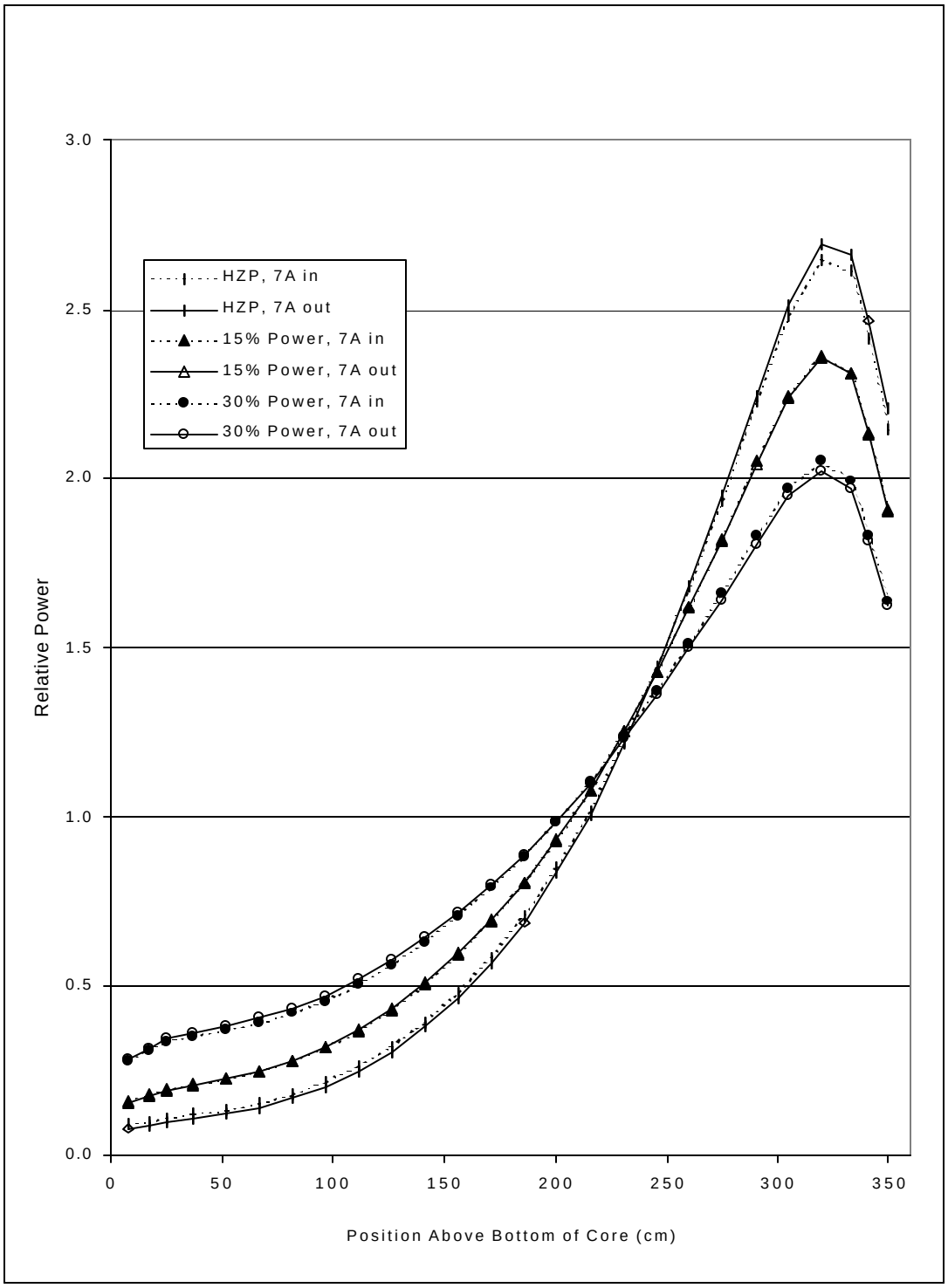

Figure 3.26 Axial normalized steady state power distributions at various power levels with bank 5 inserted

0.228	1.130	1.241	1.431	0.655	0.903	0.432	0.324	7a in
2.101	***2.676***	***1.905***	***1.744***	***0.666***	***0.782***	***0.340***	***0.244***	***7a out***
	1.053	1.404	1.179	1.259	0.664	1.049	0.441	
	2.004	***2.031***	***1.368***	***1.227***	***0.559***	***0.809***	***0.331***	
		0.727	1.293	1.156	1.457	1.259	0.459	
		0.905	***1.340***	***1.034***	***1.168***	***0.956***	***0.342***	
			0.703	1.362	1.190	0.904		
			0.644	***1.121***	***0.919***	***0.676***		
				0.818	1.312	0.618		
				0.633	***0.978***	***0.454***		
					0.763			
					0.558			

Figure 3.27 Radial normalized steady state power distributions at HZP with bank 5 inserted

0.228	1.121	1.227	1.417	0.655	0.912	0.440	0.330	7a in
1.897	***2.431***	***1.764***	***1.663***	***0.660***	***0.809***	***0.362***	***0.263***	***7a out***
	1.043	1.391	1.169	1.256	0.668	1.061	0.449	
	1.833	***1.897***	***1.315***	***1.224***	***0.580***	***0.863***	***0.357***	
		0.724	1.287	1.150	1.457	1.266	0.466	
		0.867	***1.320***	***1.048***	***1.221***	***1.019***	***0.369***	
			0.703	1.359	1.189	0.910		
			0.653	***1.163***	***0.969***	***0.724***		
				0.819	1.315	0.624		
				0.669	***1.044***	***0.490***		
					0.768			
					0.601			

Figure 3.28 Radial normalized steady state power distributions at 15% power with bank 5 inserted

0.229	1.115	1.214	1.405	0.656	0.921	0.447	0.336
1.768	***2.274***	***1.672***	***1.608***	***0.657***	***0.828***	***0.378***	***0.277***
	1.034	1.379	1.160	1.253	0.673	1.072	0.457
	1.724	***1.809***	***1.279***	***1.221***	***0.596***	***0.900***	***0.376***
		0.723	1.282	1.144	1.455	1.272	0.473
		0.843	***1.306***	***1.055***	***1.253***	***1.060***	***0.388***
			0.704	1.356	1.187	0.915	
			0.660	***1.187***	***0.999***	***0.755***	
				0.820	1.317	0.629	
				0.692	***1.086***	***0.513***	
					0.773		
					0.630		

7a in
7a out

Figure 3.29 Radial normalized steady state power distributions at 30% power with bank 5 inserted

0.229	1.115	1.214	1.405	0.656	0.921	0.447	0.336
1.768	*2.274*	*1.672*	*1.608*	*0.657*	*0.828*	*0.378*	*0.277*
2.041	**2.592**	**1.836**	**1.696**	**0.664**	**0.803**	**0.357**	**0.259**
2.101	***2.676***	***1.905***	***1.744***	***0.666***	***0.782***	***0.340***	***0.244***
	1.034	1.379	1.160	1.253	0.673	1.072	0.457
	1.724	*1.809*	*1.279*	*1.221*	*0.596*	*0.900*	*0.376*
	1.935	**1.968**	**1.334**	**1.220**	**0.572**	**0.843**	**0.350**
	2.004	***2.031***	***1.368***	***1.227***	***0.559***	***0.809***	***0.331***
		0.723	1.282	1.144	1.455	1.272	0.473
		0.843	*1.306*	*1.055*	*1.253*	*1.060*	*0.388*
		0.890	**1.325**	**1.030**	**1.184**	**0.987**	**0.360**
		0.905	***1.340***	***1.034***	***1.168***	***0.956***	***0.342***
			0.704	1.356	1.187	0.915	
			0.660	*1.187*	*0.999*	*0.755*	
			0.648	**1.131**	**0.934**	**0.700**	
			0.644	***1.121***	***0.919***	***0.676***	
				0.820	1.317	0.629	
				0.692	*1.086*	*0.513*	
				0.648	**1.004**	**0.474**	
				0.633	***0.978***	***0.454***	
					0.773		
					0.630		
					0.580		
					0.558		

30% 7a in (ss)
30% 7a out (ss)
30% rho max (trans)
HZP 7a out (ss)

Figure 3.30 Comparison of normalized radial power distribution with bank 5 inserted

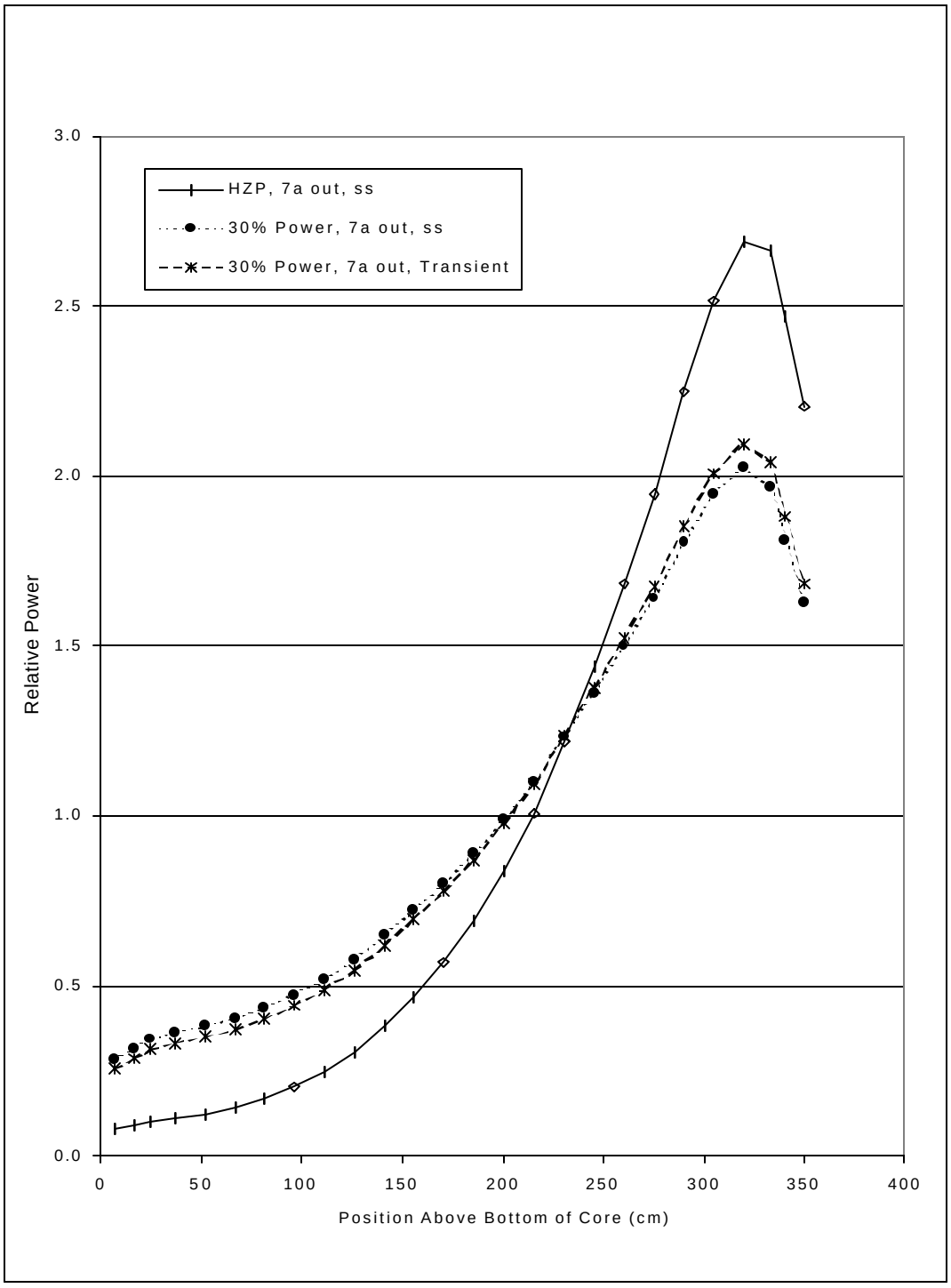

Figure 3.31 Comparison of normalized axial power distributions with bank 5 inserted

The steady-state normalized axial power distributions computed by PARCS for EOC at various power levels with control bank 5 fully withdrawn, and rod 7A fully inserted or withdrawn show the same trends found in Figure 3.26 for the same situation with bank 5 inserted. Power peaking in the top of the core becomes more damped as core power level increases and the axial power distribution is similar independent of whether rod 7A is inserted or withdrawn. Furthermore, it is found that the axial distribution for the HZP case is almost identical with bank 5 withdrawn or inserted.

The steady-state normalized radial power distributions computed by PARCS for EOC at various power levels with control bank 5 fully withdrawn, and rod 7A fully inserted or withdrawn are shown in Figures 3.32 to 3.34 and should be compared with Figures 3.27 to 3.29. With bank 5 withdrawn, the radial power distributions at all power levels with rod 7A fully inserted are only slightly different. For example, the relative power in the central fuel assembly is 0.154 at HZP, and 0.161 at 30% power, a 4.5% difference. Comparisons of all other fuel assemblies show that there is only a small change in the power distribution with rod 7A fully inserted as the power level is increased from HZP to 30% power. Similarly, the power distributions at various power levels are quite comparable with rod 7A fully withdrawn. For example, the relative power in the central fuel assembly is 1.21 at HZP, and 1.16 at 30% power, a 5% difference.

In comparison with the normalized radial power distributions with Bank 5 fully inserted, the power distributions with Bank 5 fully withdrawn are much flatter. When Bank 5 is withdrawn, the neutron flux and power distributions are shifted outwards in the radial direction. Any perturbations near the center of the core will have less of an impact on the flux and power distributions and hence, the effective worth of control rod 7A is reduced significantly at elevated power levels.

0.154	0.779	0.916	1.192	0.693	1.231	0.544	0.363	7A in
1.213	***1.588***	***1.239***	***1.332***	***0.685***	***1.137***	***0.489***	***0.321***	***7A out***
	0.743	1.071	1.029	1.351	1.194	1.264	0.478	
	1.225	***1.372***	***1.111***	***1.313***	***1.096***	***1.130***	***0.423***	
		0.631	1.304	1.206	1.581	1.318	0.466	
		0.713	***1.316***	***1.141***	***1.435***	***1.173***	***0.412***	
			1.131	1.415	1.122	0.838		
			1.083	***1.305***	***1.007***	***0.743***		
				0.767	1.133	0.526		
				0.692	***1.005***	***0.464***		
					0.631			
					0.556			

Figure 3.32 Normalized steady state radial power distributions at HZP with bank 5 withdrawn

0.158	0.792	0.924	1.196	0.693	1.229	0.546	0.365	7A in
1.183	***1.552***	***1.217***	***1.318***	***0.684***	***1.142***	***0.496***	***0.327***	***7A out***
	0.753	1.080	1.030	1.346	1.187	1.263	0.482	
	1.199	***1.352***	***1.100***	***1.309***	***1.098***	***1.141***	***0.431***	
		0.636	1.301	1.197	1.570	1.315	0.469	
		0.708	***1.309***	***1.136***	***1.437***	***1.183***	***0.419***	
			1.126	1.408	1.118	0.841		
			1.081	***1.307***	***1.014***	***0.754***		
				0.767	1.136	0.531		
				0.699	***1.019***	***0.474***		
					0.636			
					0.567			

Figure 3.33 Normalized steady state radial power distributions at 15% power with bank 5 withdrawn

0.161	0.803	0.930	1.198	0.693	1.228	0.549	0.368	7A in
1.160	***1.524***	***1.200***	***1.307***	***0.683***	***1.146***	***0.501***	***0.332***	***7A out***
	0.761	1.087	1.030	1.341	1.181	1.262	0.485	
	1.180	***1.337***	***1.092***	***1.305***	***1.098***	***1.150***	***0.438***	
		0.640	1.299	1.189	1.560	1.312	0.473	
		0.706	***1.303***	***1.132***	***1.438***	***1.191***	***0.426***	
			1.121	1.401	1.115	0.843		
			1.078	***1.307***	***1.019***	***0.762***		
				0.768	1.140	0.536		
				0.704	***1.031***	***0.482***		
					0.642			
					0.577			

Figure 3.34 Normalized steady state radial power distributions at 30% power with bank 5 withdrawn

4. SUMMARY AND CONCLUSIONS

The objective of this study was to study the rod ejection accident in order to understand sources of uncertainty in calculating the fuel enthalpy throughout the core and to provide information useful for designing experimental programs to test fuel under REA conditions. The PARCS code was used to carry out transient three-dimensional simulations of REAs using a model of the core of the TMI-1 PWR. Base case initial conditions were HZP for both BOC and EOC. The EOC model was based on a benchmark problem and had substantial validation.

The model was altered to run numerous parametric studies. In order to do studies with a range of control rod worths, the worth of the central control rod was artificially changed by multiplication factors on the absorption and fission yield cross sections of the fuel assembly. This procedure permitted control rod worths in excess of prompt-critical (ρ > \$1.0) in order to test the effect of variations in other items such as delayed neutron fraction, heat transfer properties, reactor trip, control rod position, and power level.

The maximum local fuel enthalpy increase during an REA varied almost linearly as a function of rod worth and delayed neutron fraction. The dependencies of the enthalpy increase with rod worth and delayed neutron fraction at EOC collapsed onto a single curve when the maximum enthalpy change was plotted against the difference between the absolute rod worth and the delayed neutron fraction. The enthalpy increase at BOC was higher than at EOC by about 5 to 10 cal/g for a given (ρ-β). The higher enthalpy rise at BOC can be explained by the higher content of fissile fuel in various assemblies, which leads to higher power densities and energy deposition in the event of an REA transient. For rod worths below \$1.5, the maximum fuel pellet enthalpy increase was less than 40 cal/g. In order to obtain fuel enthalpies of ~100 cal/g it would be necessary to have a rod worth of ~\$2.7 at EOC nominal conditions, something not considered credible. Rod worths above prompt-critical are possible but the probability of a given worth diminishes at higher worths.

The pulse widths of the power transients in the REA simulations by PARCS were shown to have inverse relationships with both the rod worth and maximum fuel pellet enthalpy increase. In congruence to the higher fuel pellet enthalpy rise at BOC, the pulse width at BOC was shorter than at EOC for a given rod worth due to the higher fissile fuel content. For rod worths varying between \$1.2 and \$2.2, the pulse width varied between 70 ms and 10 ms. The implication of these observations re designing an experiment to capture the limiting situation, namely, a fuel enthalpy increase of ~100 cal/g, is that the pulse width should be ~10 ms.

A comparison with the zero-dimensional analytical Nordheim-Fuchs model for super-prompt critical adiabatic reactor transients with linear negative temperature feedback demonstrated that the comprehensive three-dimensional PARCS simulation produced the same trends suggested by the simpler analytical model. The Nordheim-Fuchs model gives a linear dependence between energy deposition and rod worth, and an inverse relationship between the pulse width and rod worth.

For a given rod worth, the location of the ejected rod has little effect on the resulting energy deposition. This is based on calculations with the ejected rod at three widely different locations in the core. Of course, the rod worth will be determined largely by its location.

Most of the studies were done with a conservative set of reactor trip parameters. The pulse width of an REA is short compared to the delay and insertion time of the shutdown control rods. Thus, most of the energy deposition occurs before scram begins to add negative reactivity. Comparing a calculation with a trip signal occurring at 0.3 s with one occurring at a time greater than 3.0 s, the difference in the maximum fuel pellet enthalpy rise is less than 2 cal/g within 3 s for a \$1.2 rod ejection.

There are several heat transfer properties which have a small effect on the outcome of the REA. The peak fuel enthalpy drops with increasing gap conductance due to improved heat transfer to the coolant, however, the effect is relatively weak. A 20% increase in the gap conductance reduces the fuel enthalpy by less than 1 cal/g for a $1.2 rod ejection. PARCS calculations show that the maximum fuel pellet enthalpy rise is directly proportional to the fuel heat capacity with a sensitivity of unity. This result is consistent with that suggested by the approximate analytical Nordheim-Fuchs model. The use of a non-uniform power distribution for the fuel pellet, which is considered to be more representative of an actual fuel pin after an extended burn-up, gives a lower enthalpy increase during an REA than using a uniform power distribution. A power distribution that is peaked towards the outer radius of the fuel pellet will result in better heat transfer to the coolant. Thus, REA calculations done with a uniform power distribution can be considered to be more conservative in a safety evaluation where fuel enthalpy is the only parameter of interest. However, if DNB is of interest, then it may be more conservative to use the peaked power distribution as this leads to an increase in heat flux relative to the case with uniform power distribution

Steady-state calculations of the worth of the central control rod with power level demonstrate that thermal-hydraulic feedback at higher power levels lowers the worth of a control rod. Transient calculations of rod worth during an REA at elevated power levels are higher than those computed by a set of steady state calculations due to the delayed effect of thermal-hydraulic feedback. As the regulating bank 5 is withdrawn, the worth of the central control rod drops due to the shift in the neutron flux distribution to the outer fuel assemblies in the core. With bank 5 withdrawn, a perturbation in the flux distribution by control rod 7A in the central fuel assembly will be less significant. Thus, an REA analysis at HZP with regulating control bank 5 fully inserted can be considered the most conservative in a safety evaluation since the central control rod will have the highest worth when ejected at these conditions.

5. REFERENCES

1. D.J. Diamond, "A Probabilistic Profile for Reactivity Accidents," Letter Report W-6382 to the U.S. Nuclear Regulatory Commission, Brookhaven National Laboratory, February 1998.

2. R.O. Meyer et al., "A Regulatory Assessment of Test Data for Reactivity-Initiated Accidents," *Nuclear Safety, 37,* October-December 1996.

3. D.J. Diamond, C.-Y. Yang, and A.L. Aronson, "Estimating the Uncertainty in Reactivity Accident Neutronic Calculations,' Proceedings of the Twenty-Sixth Water Reactor Safety Information Meeting, October 1998, NUREG/CP-0166, U.S. Nuclear Regulatory Commission, March 1999.

4. A. Avvakumov, V. Malofeev, and V. Sidorov, "Analysis of Pin-by-Pin Effects for LWR Rod Ejection Accident," Russian Research Centre - Kurchatov Institute, NUREG/IA-0175, U.S. Nuclear Regulatory Commission, March 2000.

5. D.J. Diamond et al., "Intercomparison of Results for a PWR Rod Ejection Accident," Proceedings of the Twenty-Seventh Water Reactor Safety Information Meeting, October 1999, NUREG/CP-0169, U.S. Nuclear Regulatory Commission, March 2000, and *Nuclear Engineering and Design, 208,* 181, 2001.

6. D.J. Diamond, A.L. Aronson, and C.-Y. Yang, "Uncertainty Analysis for the PWR Rod Ejection Accident," *Trans. Amer. Nucl. Soc., 83,* November 2000.

7. H.G. Joo et al., "PARCS: A Multi-Dimensional Two-Group Reactor Kinetics Code Based on the Non-linear Analytic Nodal Method," PU/NE-98-26, Purdue University, School of Nuclear Engineering, September 1998.

8. K.N. Ivanov et al., "PWR Main Steam Line Break (MSLB) Benchmark; Volume I: Final Specifications," NEA/NSC/DOC(99)8, U.S. Nuclear Regulatory Commission and OECD Nuclear Energy Agency, April 1999.

9. D.T. Hagrman, editor, "SCADAP/RELAP5/MOD 3.1 Code Manual Volume 4: MATPRO – a library of Materials Properties for Light-Water-Reactor Accident Analysis," NUREG/CR-6150, U.S. Nuclear Regulatory Commission, 1995.

10. A. Avvakumov, Russian Research Centre - Kurchatov Institute, Private Communication to David Diamond, Brookhaven National Laboratory, February 28 and July 4, 2001.

11. David L. Hetrick, Dynamics of Nuclear Reactors, American Nuclear Society, La Grange Park, Illinois, U.S.A., Chapter 5, pp. 164-170, 1993.

12. J.J. Duderstadt and L.J. Hamilton, Nuclear Reactor Analysis, John Wiley and Sons, New York, Chapter 10, pp. 398-426, 1976.

13. K. Lassmann, C. O'Carroll, J. van de Laar, and C.T. Walker, "The Radial Distribution of Plutonium in High Burn-up UO2 Fuels," *Journal of Nuclear Materials, 208,* pp. 223-231, 1994.

14. H. Carlsen and D.N. Sah, “Radial Concentration and Effect on Temperature of Plutonium Formed In UO2 During Irradiation,” *Nuclear Technology*, *55*, pp. 587-593, 1981.

15. Schwencer, Atomic Energy Commission, Light Water Reactors Branch, “Arkansas Unit 1 PWR Operating License Number DPR-5 with Technical Specifications,” Figure 3.5.2-1, page 48b, Amendment 92, 1974.